THE ASTROPHYSICAL JOURNAL, 458:435–454, 1996 February 20

STRUCTURE AND DYNAMICS OF THE COMA CLUSTER

MATTHEW COLLESS[1]
Mount Stromlo and Siding Spring Observatories, Australian National University, Weston Creek, ACT 2611, Australia
AND
ANDREW M. DUNN
Institute of Astronomy, Madingley Road, Cambridge CB3 0HA, UK
Received 1995 May 31; accepted 1995 August 22

ABSTRACT

We examine the structure and dynamics of the galaxies in the Coma cluster using a catalog of 552 redshifts including 243 new measurements obtained with the Hydra multifiber spectrograph at KPNO. The velocity distribution for the 465 cluster members is clearly non-Gaussian. A new test for localized variations in the velocity distribution shows highly significant structure associated with the group of galaxies around NGC 4839, 40′ SW of the cluster core. We apply a mixture-modeling algorithm to the galaxy sample and obtain a robust partition into two subclusters: the main Coma cluster centered on NGC 4874, with $\overline{cz} = 6853$ km s^{-1} and $\sigma_{cz} = 1082$ km s^{-1}, and a group centered on NGC 4839, with $\overline{cz} = 7339$ km s^{-1} and $\sigma_{cz} = 329$ km s^{-1}.

We use this partition to examine the system's dynamics. We find that the velocity dispersion of the late-type galaxies in the main cluster is very close to $2^{1/2}$ times that of the early-type galaxies, suggesting that the late types are freely falling into a largely virialized cluster core dominated by early types. We obtain a virial mass for the main cluster of $0.9 \times 10^{15}\ h^{-1}\ M_{\odot}$, in close agreement with the estimates derived from recent X-ray data. The mass of the NGC 4839 group is found to be $0.6 \times 10^{14}\ h^{-1}\ M_{\odot}$, or about 5%–10% the mass of the main cluster, in accord with their relative richnesses and X-ray luminosities. Assuming the main cluster and the NGC 4839 group follow a linear two-body orbit, the favored solution has the two clusters lying at 74° to the line of sight at a true separation of $0.8\ h^{-1}$ Mpc and moving together at 1700 km s^{-1}.

Closer examination of the cluster core reveals an ongoing merger between two subclusters centered in projection on the dominant galaxies NGC 4874 and NGC 4889 but offset in velocity by 300 and 1100 km s^{-1}, respectively. Combining these results with X-ray and radio observations, and an interpretation of the presence or lack of an extended halo around the dominant galaxies NGC 4874, NGC 4889, and NGC 4839, we develop a merger history for the Coma cluster. We suggest that the cD NGC 4839 is at the center of the group in which it formed, and that this group is just beginning to penetrate the Coma cluster, into which it is falling from the direction of Abell 1367 along the Great Wall. We argue that the radio halo of Coma and the disturbed X-ray emission in its core are the result of the ongoing merger between the main cluster and a group dominated by NGC 4889. This group has now been partially disrupted, ejecting NGC 4889. The position and apparent halo of NGC 4874 indicate that it was the original dominant galaxy of the main Coma cluster, though it may now have been dislodged from the bottom of the potential well.

Subject headings: galaxies: clusters: individual (Coma) — galaxies: distances and redshifts — galaxies: elliptical and lenticular, cD — galaxies: kinematics and dynamics

1. INTRODUCTION

It is no longer possible to use Coma as the exemplar of a rich, regular, and relaxed galaxy cluster. Studies of the projected distributions of both the galaxies and the X-ray gas show convincing evidence of statistically significant substructures on both large and small scales, although evidence for substructure in the galaxy velocity distribution has been slight at best. In this paper we use new measurements of galaxy redshifts in Coma to demonstrate that the main structures visible in the projected maps are also identifiable in velocity space. We also take some initial steps toward understanding the dynamical significance of the observed substructure, and propose an outline of the merger history of the Coma cluster.

The most detailed and convincing evidence for substructure in Coma comes from the X-ray images obtained with *ROSAT*. Briel, Henry, & Böhringer (1992) construct a map of Coma using the *ROSAT* all-sky survey data, which shows that the contours of the X-ray emission in the cluster core are elongated along the line joining the two central dominant galaxies, NGC 4874 and NGC 4889. The map also shows a secondary peak, accounting for 6% of the total cluster emission, around the group of galaxies centered on the cD galaxy NGC 4839, 40′ to the SW of the cluster core. A much deeper *ROSAT* image published by White, Briel, & Henry (1993) confirms these structures and suggests lower level clumps of emission associated with a few of the other bright cluster galaxies.

The main structures seen in these X-ray maps had already been detected in the projected distribution of galaxies. Fitchett & Webster (1987) demonstrate the existence of double structure in the cluster core, with two clumps of galaxies centered on NGC 4874 and NGC 4889, while Mellier et al. (1988) use the color-magnitude relation for early-type galaxies to select probable cluster members and show that the large-scale galaxy distribution has a second peak around NGC 4839. Merritt & Tremblay (1994) apply an adaptive kernel method to obtain an improved map of the galaxy distribution based on the Mellier et al. sample. A good summary of the evidence for substructure

[1] Visiting Astronomer, Kitt Peak National Observatory. KPNO is operated by AURA, Inc., under contract to the National Science Foundation.

in Coma prior to the *ROSAT* maps is given by Baier, Fritze, & Tiersch (1990).

Although structure is clearly apparent in the projected galaxy distribution, it is not so apparent in the distribution of radial velocities. Fitchett & Webster (1987) find only weak evidence of velocity structure associated with the two clumps they identify in the cluster core. Merritt (1987) notes that the velocity distribution of galaxies *outside* the cluster core is significantly skew, but the Dressler & Shectman (1988) test for localized departures from a Gaussian velocity distribution does not reveal any significant substructures.

This paper takes up the issue of velocity structure in the Coma cluster, inspired and guided by the beautiful *ROSAT* images. The analysis is based on a catalog of galaxy positions, magnitudes, colors, and redshifts compiled from various sources in the literature, to which we have added more accurate positions and new redshifts for 243 galaxies. We use this catalog to examine the cluster's line-of-sight velocity distribution and find highly significant departures from a single Gaussian. Applying a powerful new test for localized velocity substructure, we are able to show that the origin of these departures is a group of galaxies centered on NGC 4839 and corresponding closely to the secondary peak in the *ROSAT* maps. We partition the galaxy sample between the main cluster and this NGC 4839 group using a maximum-likelihood algorithm, and derive mean velocities, velocity dispersions, and masses for both subclusters. We model the dynamics of this system with a simple two-body model and obtain a favored solution supported by existing optical, X-ray, and radio data. Looking for structure on smaller scales, we show the existence of velocity substructure associated with the two dominant galaxies NGC 4874 and NGC 4889 in the cluster core. Finally we attempt to synthesize all the available information on the structure and dynamics into a coherent picture of the merger history of the Coma cluster.

2. DATA

2.1. *The Coma Redshift Catalog*

Godwin, Metcalfe, & Peach (1983, hereafter GMP) list 6724 galaxies brighter than $b = 21$ in a square region of side 2°.63 (3.0 h^{-1} Mpc) centered on the Coma cluster ($\alpha = 12^h59^m42^s.8$, $\delta = +27°58'14''$, J2000). The GMP sample is complete to $b = 20$, at which limit it includes 2510 galaxies. Our catalog is based on this complete subsample of the GMP data.

The b passband of GMP is defined by the combination of a IIIa–J emulsion and a Wr2C filter, zero-pointed with photoelectric B-band observations of 96 of the brighter galaxies. The b-magnitudes are integrated within the $\mu_b = 26.5$ mag arcsec^{-2} isophote. The r passband is defined by the combination of a 127-04 emulsion and an RG1 filter, with a zero point giving $b-r \approx B-R$. The r-magnitudes are integrated within the $\mu_r = 24.75$ mag arcsec^{-2} isophote. GMP claim external errors in b, r, and $b-r$ of approximately 0.15 mag.

The GMP catalog gives positions with a rms uncertainty of approximately 2″. This is inadequate for positioning fibers, so the GMP catalog was matched with the positions obtained from a UK Schmidt Telescope plate (J10027) scanned with the APM measuring machine at the Royal Greenwich Observatory. The APM positions have a rms uncertainty of less than 1″. Of the 2510 galaxies in the GMP catalog 2348 (94%) could be satisfactorily matched to an APM galaxy. Of the remaining 162 galaxies, 48 could not be matched within 6″ (roughly the joint 3 σ uncertainty) and so the GMP position was kept, while in another 114 cases the match was doubtful because of a large difference between the GMP and APM magnitudes or because APM classed the object as a star or junk. Most of the cases of no or doubtful matching between the GMP and APM objects were fainter than $b = 19$. The final set of positions were transformed from B1950 to J2000.

A near-complete set of redshifts from the literature were then obtained for the galaxies in this sample by searching the NED[2] database (as at 1993 October 1). Further redshifts were added to this list from Kent & Gunn (1982), van Haarlem et al. (1993), and Caldwell et al. (1993). The total number of redshifts found in this way was 345.

2.2. *New Redshift Measurements*

In order to supplement the literature observations, particularly in the regions of interest indicated by the *ROSAT* observations, we used the Hydra fiber spectrograph on the KPNO 4 m telescope to measure new redshifts. The 40′ diameter Hydra fields we observed are shown in Figure 1, together with the GMP galaxies brighter than $b = 20$ and the X-ray contours from White et al. (1993). Within each field we observed the brightest galaxies with $b < 20$ that had no previous redshift measurement, plus a control sample of galaxies with known redshift.

The observations were made on 1992 March 8–10. Although most of the first two nights were lost to snow, we obtained 1.5–2 hr of integration on each of four fields. Spectra were obtained over 3700–5700 Å with a 632 lines mm^{-1} grating (KPC-007A) and Tektronix 2048^2 CCD (T2KB), giving a resolution of 1.0 Å pixel^{-1} and 4.2 Å FWHM. The data were reduced using the standard IRAF tasks ccdproc and dohydra. Redshifts were obtained using the cross-correlation task xcsao for absorption-line objects and for emission-line objects by Gaussian fits to the line profiles.

The new redshifts are listed in Table 1. For each galaxy we give the GMP catalog number, the J2000 position, the b-magnitude, and $b-r$ color from GMP, the heliocentric redshift cz and its uncertainty Δcz in km s^{-1}, the Tonry & Davis (1979) R-value for the cross-correlation (for absorption-line spectra), a quality code Q for the redshift measurement (described below), and the number of emission lines E (if present).

The quality code was assigned to each redshift on the basis of visual inspection of both the spectrum and the cross-correlation function: $Q = 0$ if no redshift identification could be made (the 110 $Q = 0$ objects are omitted from Table 1); $Q = 1$ if a cross-correlation redshift was obtained but was not certain (57 objects); $Q = 2$ if the cross-correlation redshift was certain (161 objects); and $Q = 9$ if a redshift was measured from emission lines (25 objects). The rms estimated uncertainties for quality codes $Q = 1$, 2, 9 are $\delta cz = 65$, 30, 52 km s^{-1}. Emission-line redshifts are considered certain if based on more than one line, as is the case for 22 of the 25 emission-line redshifts. As Figure 2 shows, the distinction between $Q = 1$ and $Q = 2$ corresponds quite closely to $R < 3$ and $R > 3$. Figure 3 shows some examples of $Q = 1$, 2, and 9 spectra, with identified features marked.

The comparison with pre-1992 literature redshifts is limited, since we specifically tried to exclude such objects. Comparing

[2] NED is the NASA/IPAC extragalactic database, operated for NASA by the Jet Propulsion Laboratory at Caltech.

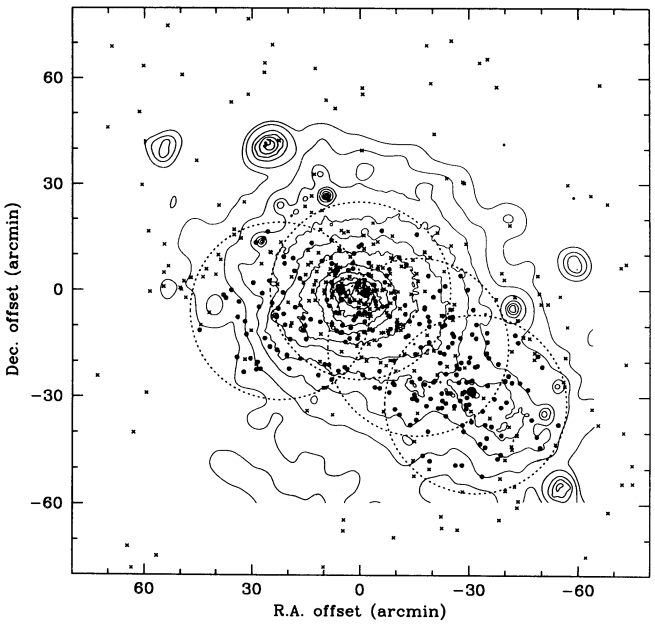

FIG. 1.—Coma cluster fields observed with Hydra (*dotted circles*) and the positions of the galaxies with redshift measurements (*dots*, new data; *crosses*, literature data), superposed on the contours of the *ROSAT* observations of White et al. (1993). The three dominant galaxies (NGC 4874, NGC 4889, and NGC 4839) are shown as larger dots.

our new results with the heterogeneous collection of redshifts found in NED, we find 15 objects in common, with a mean velocity difference of 25 km s^{-1} and a rms scatter of 122 km s^{-1} (see Fig. 4*a*). A better external estimate of our velocity errors can be obtained from the 45 galaxies we have in common with the high-quality velocity measurements obtained by Caldwell et al. (1993). In this comparison we find an approximately Gaussian distribution for Δcz with a slight offset in the mean of -22 km s^{-1} and a rms scatter of only 48 km s^{-1}, consistent with the quoted rms uncertainties (see Fig. 4*b*). However, these comparisons only apply to the brighter galaxies in our sample—all the objects involved are brighter than $b = 19$ and have quality codes of either $Q = 2$ or $Q = 9$. The comparisons confirm the accuracy of the redshifts we consider certain, but provide no check on the less certain $Q = 1$ measurements. Such a check is provided by some redshift measurements kindly communicated in advance of publication by Biviano et al. (1995). Of 52 objects in common, five have discrepancies of more than 500 km s^{-1} (GMP numbers 3080, 3768, 4659, 4749, and 4825). The remaining 47 objects have a mean offset of -34 km s^{-1} and a rms scatter of 125 km s^{-1}, dominated by the estimated error of approximately 100 km s^{-1} given by Biviano et al. for their velocities (see Fig. 4*c*). Of the five discrepant objects, four have reliable ($Q = 2$ or 9) ratings in our catalog but low quality ratings in the Biviano et al. catalog, so we presume the error to lie in their estimates. Encouragingly, only one of the 12 $Q = 1$ objects in the comparison has a discrepant redshift. We, therefore, conclude that our new redshifts are generally reliable to within the quoted errors.

To summarize, we have measured a total of 243 redshifts in the GMP region about the Coma cluster. These new measurements bring the total number of redshifts in the region around Coma to 552, making it by far the best-observed cluster in the sky. The following sections employ this redshift catalog to examine the structure and dynamics of the cluster.

3. CLUSTER STRUCTURE

3.1. *Velocity Distribution*

The line-of-sight distribution of cz for the galaxies in our redshift catalog is shown in Figure 5. If we determine cluster membership using pessimistic 3 σ clipping (Colless & Hewett 1987), we find there are 465 galaxies in the cluster, which spans the range 4000–10,000 km s^{-1}. The mean and standard devi-

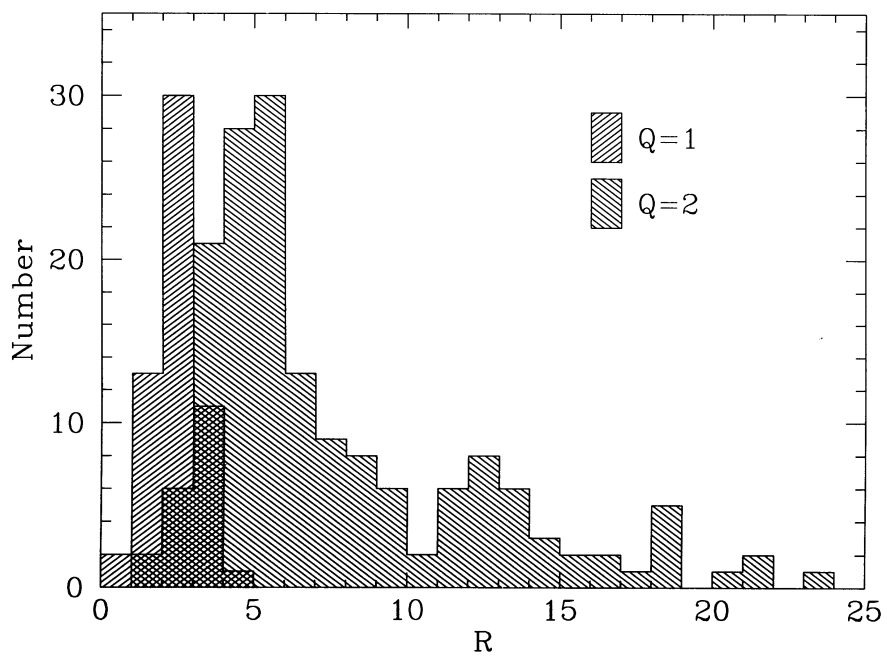

FIG. 2.—Distributions of the Tonry & Davis R parameter for objects with quality codes $Q = 1$ and $Q = 2$. The difference between $Q = 1$ and $Q = 2$ corresponds approximately to $R = 3$.

TABLE 1

CATALOG OF NEW REDSHIFTS

GMP	(J2000) α	(J2000) δ	b	$b-r$	cz	δcz	R	Q	E
1134.....	$13^h03^m05^s.16$	+27°47′02″.5	16.69	1.90	7666	104	2.1	1	...
1397.....	13 02 34.75	+27 56 57.1	16.31	1.83	5779	12	14.3	2	...
1425.....	13 02 31.84	+27 56 07.7	17.37	1.79	6637	18	8.8	2	...
1471.....	13 02 24.97	+27 58 20.2	19.11	1.70	7154	56	1.6	1	...
1535.....	13 02 17.82	+27 39 32.3	18.71	1.34	21222	47	...	9	1
1543.....	13 02 16.84	+27 50 44.1	19.97	1.85	7651	34	3.2	1	...
1555.....	13 02 15.28	+27 55 03.1	19.10	2.52	48346	60	4.7	2	...
1599.....	13 02 09.31	+27 35 21.2	18.45	1.80	6444	28	5.0	2	...
1617.....	13 02 07.73	+27 49 30.9	19.99	2.11	59968	56	0.8	1	...
1636.....	13 02 05.97	+27 45 54.1	18.71	1.91	7251	23	6.0	2	...
1673.....	13 02 01.02	+27 39 10.1	16.53	1.86	7102	12	14.8	2	...
1715.....	13 01 57.30	+28 00 20.9	14.95	2.09	7735	20	14.4	2	...
1751.....	13 01 54.09	+28 11 38.4	17.79	1.79	28837	66	2.4	1	...
1756.....	13 01 53.52	+27 36 03.5	19.11	1.98	47535	61	...	9	1
1775.....	13 01 52.02	+27 38 09.4	18.31	1.36	17437	27	...	9	4
1807.....	13 01 50.17	+27 53 36.5	15.77	1.94	7556	13	17.9	2	...
1832.....	13 01 48.35	+27 36 14.0	16.59	1.84	8223	11	13.9	2	...
1865.....	13 01 46.05	+27 57 26.7	17.09	2.13	4706	13	13.4	2	...
1885.....	13 01 44.14	+28 12 51.3	17.65	1.78	7802	15	10.7	2	...
1895.....	13 01 42.84	+27 44 51.0	17.52	1.36	10614	59	...	9	5
1931.....	13 01 39.03	+28 14 45.1	18.11	1.69	7599	29	4.9	2	...
1953.....	13 01 37.30	+28 00 56.6	18.66	1.82	7179	25	5.9	2	...
1961.....	13 01 36.50	+27 42 28.2	18.03	1.88	7915	19	6.8	2	...
1986.....	13 01 33.80	+27 54 39.9	17.91	1.78	6327	58	2.6	1	...
2035.....	13 01 28.12	+27 51 06.2	18.47	1.28	72914	137	...	9	5
2039.....	13 01 27.75	+27 41 35.2	19.91	2.52	63910	71	3.5	2	...
2059.....	13 01 26.11	+27 53 09.5	13.53	...	5481	13	18.3	2	...
2129.....	13 01 19.97	+27 57 39.2	18.78	1.84	7891	40	3.4	1	...
2141.....	13 01 19.30	+27 51 37.5	17.78	1.44	8220	33	3.9	2	...
2145.....	13 01 19.02	+28 07 41.0	18.06	1.73	6834	36	5.1	2	...
2157.....	13 01 17.56	+27 48 32.8	15.06	1.92	7282	12	20.2	2	...
2158.....	13 01 17.82	+28 05 49.0	18.66	1.75	8030	30	4.1	2	...
2185.....	13 01 15.19	+27 40 08.8	17.69	1.87	7085	16	8.9	2	...
2219.....	13 01 12.27	+27 36 15.8	16.73	1.93	7513	14	12.5	2	...
2232.....	13 01 11.19	+27 44 33.0	19.13	1.73	7383	54	2.8	1	...
2270.....	13 01 07.32	+28 07 17.6	18.88	1.73	104000	100	...	9	1
2289.....	13 01 05.62	+28 03 43.4	18.43	1.60	7405	26	4.4	2	...
2295.....	13 01 04.79	+27 53 30.1	18.37	1.89	5774	51	3.5	2	...
2353.....	13 00 58.78	+28 01 36.4	19.11	1.60	42190	52	2.1	1	...
2355.....	13 00 58.36	+27 39 07.3	16.56	1.81	5233	16	9.7	2	...
2385.....	13 00 54.73	+27 50 31.2	17.62	1.82	7092	17	9.6	2	...
2393.....	13 00 54.03	+27 47 00.8	16.51	1.90	8305	15	12.0	2	...
2411.....	13 00 52.47	+27 48 17.6	18.83	1.82	6966	67	2.3	1	...
2421.....	13 00 51.08	+27 44 34.6	17.98	1.90	8112	34	4.0	2	...
2478.....	13 00 45.39	+27 50 07.9	18.09	1.86	8765	22	6.0	2	...
2501.....	13 00 43.90	+28 11 31.9	19.60	...	56861	45	4.1	2	...
2582.....	13 00 35.69	+27 34 27.0	16.20	1.74	5097	25	6.6	2	...
2603.....	13 00 33.33	+27 49 26.9	17.36	1.80	8181	16	7.9	2	...
2626.....	13 00 30.94	+28 06 30.0	18.89	1.68	5203	47	3.5	1	...
2659.....	13 00 27.63	+27 37 30.3	18.05	1.92	5876	23	6.7	2	...
2692.....	13 00 24.79	+27 55 35.6	18.20	1.78	7955	43	3.5	2	...
2721.....	13 00 22.35	+27 37 24.2	17.50	1.82	7579	23	6.0	2	...
2736.....	13 00 21.64	+27 53 54.6	18.21	1.76	4890	42	4.9	2	...
2776.....	13 00 19.09	+27 33 13.1	16.17	1.89	5891	20	8.7	2	...
2777.....	13 00 18.85	+28 00 33.3	18.21	1.71	6202	22	5.8	2	...
2783.....	13 00 18.55	+27 48 55.4	17.37	1.83	5294	33	5.1	2	...
2784.....	13 00 18.51	+28 05 49.3	18.36	1.81	7838	49	2.7	1	...
2852.....	13 00 13.60	+27 52 01.7	17.80	1.79	7451	27	4.4	2	...
2856.....	13 00 13.39	+28 03 11.5	18.23	1.57	8135	38	3.0	1	...
2866.....	13 00 12.60	+27 46 54.5	16.90	1.79	6978	15	9.4	2	...
2879.....	13 00 11.12	+28 03 54.5	18.05	1.75	7387	26	2.7	1	...
2887.....	13 00 10.74	+27 59 26.8	19.23	...	23078	41	...	9	4
2894.....	13 00 10.38	+27 35 41.7	17.15	1.84	5589	24	6.0	2	...
2914.....	13 00 08.71	+28 09 35.1	17.18	1.81	7447	41	2.6	1	...
2923.....	13 00 08.00	+27 46 23.4	17.65	...	8664	51	2.9	1	...
2929.....	13 00 07.44	+27 57 28.6	18.66	1.90	6267	44	3.5	1	...
2931.....	13 00 07.08	+27 55 51.1	19.20	1.89	7726	37	2.6	1	...
2945.....	13 00 06.07	+27 46 30.8	16.15	1.77	6223	26	5.8	2	...
2952.....	13 00 05.66	+27 55 34.7	18.72	1.66	13272	41	2.0	1	...
2956.....	13 00 05.50	+27 48 27.2	16.20	1.98	6568	10	18.7	2	...
2964.....	13 00 05.15	+27 58 35.8	17.74	...	7792	43	1.9	1	...
2985.....	13 00 03.70	+27 57 52.4	17.87	1.65	5291	81	3.3	1	...

TABLE 1—*Continued*

GMP	(J2000) α	(J2000) δ	*b*	*b* − *r*	*cz*	δ*cz*	*R*	*Q*	*E*
2999.....	13 00 02.39	+27 36 45.5	18.39	1.52	33849	33	...	9	2
3012.....	13 00 01.49	+27 43 50.4	17.49	1.83	8064	48	3.5	2	...
3038.....	12 59 59.24	+27 36 11.4	19.43	1.27	6635	63	1.6	1	...
3058.....	12 59 57.59	+28 03 54.0	17.71	1.78	5798	23	5.2	2	...
3071.....	12 59 56.15	+27 44 47.2	17.17	1.18	8865	62	2.6	2	...
3080.....	12 59 55.68	+27 55 03.4	19.60	1.85	6677	49	2.2	2	...
3092.....	12 59 54.84	+27 47 45.3	17.55	1.59	8247	17	8.3	2	...
3113.....	12 59 51.74	+28 05 54.4	17.82	1.81	7601	24	5.3	2	...
3121.....	12 59 51.45	+28 04 24.1	17.34	1.76	7457	25	4.4	1	...
3126.....	12 59 50.98	+27 49 58.4	17.55	1.82	7905	18	8.5	2	...
3129.....	12 59 50.28	+28 08 39.2	17.94	1.71	6729	36	4.8	2	...
3149.....	12 59 48.51	+27 50 51.5	19.79	2.45	49551	105	1.8	1	...
3166.....	12 59 46.91	+27 59 30.8	18.37	1.79	8360	43	2.9	1	...
3176.....	12 59 46.28	+27 44 46.1	18.29	1.23	9811	98	1.0	1	...
3204.....	12 59 44.12	+28 10 34.4	18.54	1.88	8212	35	3.7	1	...
3205.....	12 59 44.20	+27 52 03.2	17.61	1.83	6196	24	6.6	2	...
3209.....	12 59 44.13	+28 00 46.8	19.37	1.66	13211	36	2.4	1	...
3245.....	12 59 40.74	+28 11 06.3	18.42	2.18	29671	158	2.1	1	...
3271.....	12 59 39.80	+27 34 35.7	16.40	1.33	5050	37	...	9	5
3298.....	12 59 37.82	+27 46 36.4	17.26	1.79	6760	31	4.1	2	...
3311.....	12 59 37.16	+27 52 13.7	18.89	1.68	6189	82	1.6	1	...
3312.....	12 59 37.00	+28 01 06.8	18.68	1.78	7293	38	3.2	2	...
3313.....	12 59 36.95	+27 49 32.7	17.53	1.83	6231	17	9.4	2	...
3383.....	12 59 31.87	+27 51 40.7	18.50	1.86	4640	34	5.5	2	...
3387.....	12 59 31.59	+28 06 01.5	18.22	1.70	7420	36	2.7	1	...
3463.....	12 59 27.29	+27 47 06.0	18.09	1.87	6618	26	4.6	2	...
3489.....	12 59 25.02	+27 59 48.1	17.93	...	5507	37	3.5	1	...
3500.....	12 59 24.58	+27 31 02.3	18.31	1.65	5882	24	5.3	2	...
3511.....	12 59 23.39	+27 55 10.3	18.80	2.00	6824	48	3.5	1	...
3585.....	12 59 18.51	+27 35 36.9	17.29	...	5779	54	1.8	1	...
3586.....	12 59 18.34	+27 42 56.7	18.18	1.81	6681	15	11.4	2	...
3588.....	12 59 18.42	+27 30 48.4	17.76	1.72	6046	23	5.6	2	...
3640.....	12 59 14.98	+28 15 03.2	17.13	...	7483	28	3.7	1	...
3645.....	12 59 14.60	+27 53 44.1	18.64	1.86	6450	21	7.1	2	...
3681.....	12 59 11.52	+28 00 33.1	18.01	1.73	6942	30	5.3	2	...
3707.....	12 59 09.45	+28 02 27.2	17.76	1.82	7220	31	5.9	2	...
3719.....	12 59 09.06	+27 53 51.0	18.29	1.91	7812	45	2.6	1	...
3765.....	12 59 06.31	+27 29 37.0	18.75	1.72	8159	35	4.2	2	...
3768.....	12 59 05.74	+28 04 13.9	18.74	1.45	10698	48	2.3	1	...
3772.....	12 59 05.51	+27 50 56.4	18.55	1.09	20074	44	...	9	4
3788.....	12 59 04.64	+27 47 30.2	18.82	1.67	25400	56	...	9	4
3829.....	12 59 01.61	+27 32 12.8	17.44	1.85	8539	19	7.8	2	...
3848.....	12 59 00.39	+27 38 38.0	19.47	1.41	8043	39	...	9	4
3853.....	12 58 59.96	+27 31 45.3	19.70	2.31	49174	86	2.0	1	...
3855.....	12 58 59.45	+27 56 04.0	18.05	1.79	5722	31	4.2	2	...
3863.....	12 58 59.38	+27 24 49.8	19.87	2.07	6584	124	1.9	1	...
3895.....	12 58 56.61	+27 49 19.1	17.74	1.72	8651	37	3.7	2	...
3898.....	12 58 56.37	+27 48 12.9	19.04	1.79	7864	64	2.4	1	...
3935.....	12 58 53.43	+28 07 33.7	16.59	1.93	7004	12	15.0	2	...
3939.....	12 58 53.79	+27 23 19.0	18.98	1.60	7654	50	2.2	1	...
4024.....	12 58 46.52	+27 54 06.3	17.97	2.39	47492	50	2.4	1	...
4029.....	12 58 46.10	+27 51 38.9	18.94	1.89	8805	32	4.4	2	...
4035.....	12 58 45.55	+27 45 13.9	18.49	1.82	6665	33	4.0	2	...
4040.....	12 58 44.51	+28 05 35.1	19.57	...	20221	61	...	9	4
4060.....	12 58 42.61	+27 45 37.6	17.57	1.31	8686	52	1.4	1	...
4083.....	12 58 40.82	+27 49 37.3	17.82	1.91	6189	20	7.4	2	...
4093.....	12 58 40.46	+27 20 27.9	17.16	1.70	20725	31	5.5	2	3
4117.....	12 58 38.39	+27 32 38.5	16.67	1.99	5973	13	12.9	2	...
4124.....	12 58 37.85	+27 27 50.0	16.77	1.71	6256	32	4.4	2	...
4155.....	12 58 35.24	+27 29 03.7	19.91	1.46	6443	38	1.2	1	...
4169.....	12 58 34.53	+27 28 09.8	19.04	1.89	33823	60	2.4	2	...
4179.....	12 58 33.75	+27 40 28.6	19.61	2.54	56567	58	4.2	2	...
4192.....	12 58 33.12	+27 21 51.3	16.32	1.88	6996	9	18.4	2	...
4206.....	12 58 32.06	+27 27 22.5	16.41	1.90	7053	9	21.3	2	...
4210.....	12 58 30.94	+28 14 00.7	17.46	1.74	7292	39	3.8	2	...
4246.....	12 58 28.88	+27 48 53.3	18.23	1.65	25377	10	...	9	3
4255.....	12 58 28.39	+27 33 33.0	16.57	1.77	7554	17	8.2	2	...
4268.....	12 58 27.08	+27 42 23.4	19.30	1.85	7001	38	4.2	2	...
4294.....	12 58 25.28	+27 11 59.5	17.64	1.72	8045	25	5.1	2	...
4310.....	12 58 22.27	+27 53 04.3	18.50	1.78	4366	28	5.3	2	...
4312.....	12 58 22.44	+27 31 55.8	19.78	1.91	4776	58	1.5	1	...
4314.....	12 58 21.99	+27 53 31.7	17.66	1.88	7337	24	6.3	2	...
4330.....	12 58 20.54	+27 25 45.6	17.96	1.67	7578	34	5.0	2	...

TABLE 1—*Continued*

GMP	(J2000) α	(J2000) δ	b	$b-r$	cz	δcz	R	Q	E
4348.....	12 58 18.21	+27 50 54.3	17.77	1.30	7576	55	2.2	2	...
4351.....	12 58 18.66	+27 18 37.9	16.85	1.52	7389	42	...	9	6
4355.....	12 58 17.39	+28 02 23.9	18.22	1.82	6205	27	6.1	2	...
4364.....	12 58 16.85	+27 43 46.6	17.42	1.77	20385	46	2.1	1	...
4366.....	12 58 16.51	+27 48 08.9	18.74	1.92	5715	30	5.4	2	...
4367.....	12 58 16.44	+27 49 36.9	17.65	2.12	25648	49	4.0	2	1
4370.....	12 58 16.95	+27 10 26.5	16.59	1.96	18179	20	11.5	2	...
4381.....	12 58 15.22	+27 27 51.6	19.27	1.96	7625	27	3.7	2	...
4420.....	12 58 11.42	+27 56 23.5	17.60	1.86	8500	20	7.5	2	...
4421.....	12 58 11.66	+27 32 32.6	19.23	1.78	7152	34	3.6	2	...
4447.....	12 58 09.68	+27 32 57.7	17.81	1.98	7002	16	10.4	2	...
4479.....	12 58 06.07	+27 25 07.7	17.51	1.83	5758	16	9.3	2	...
4502.....	12 58 03.52	+27 40 56.3	18.02	1.95	7212	13	13.1	2	...
4503.....	12 58 03.12	+27 58 13.7	16.83	1.85	20631	49	3.8	2	...
4506.....	12 58 03.44	+27 37 59.6	17.15	2.08	20376	21	12.9	2	...
4522.....	12 58 01.54	+27 29 22.5	15.83	1.84	7648	8	21.9	2	...
4530.....	12 58 01.37	+27 25 14.5	18.04	1.26	20912	38	...	9	5
4531.....	12 58 00.68	+27 48 11.7	19.00	2.41	33602	36	6.7	2	...
4535.....	12 58 00.75	+27 27 14.2	17.90	1.95	7691	15	12.0	2	...
4539.....	12 57 59.87	+27 51 08.8	19.21	1.83	7171	41	3.4	2	...
4557.....	12 57 58.22	+27 40 30.1	19.69	1.86	5291	49	3.1	2	...
4566.....	12 57 57.23	+27 48 33.4	17.74	1.57	33683	50	4.6	2	...
4570.....	12 57 56.68	+27 59 29.8	17.25	1.07	4605	10	...	9	4
4577.....	12 57 56.51	+27 26 33.5	18.43	1.44	7724	48	...	9	4
4578.....	12 57 56.50	+27 22 55.9	18.04	1.80	5193	22	6.7	2	...
4579.....	12 57 56.24	+27 34 52.2	16.72	...	4999	23	...	9	5
4597.....	12 57 54.38	+27 29 26.0	16.37	1.91	5003	24	6.7	2	...
4602.....	12 57 53.13	+27 42 25.9	18.15	1.87	6444	26	3.9	2	...
4624.....	12 57 50.92	+27 50 45.7	19.84	2.56	57238	56	3.6	1	...
4630.....	12 57 50.75	+27 29 27.0	18.97	1.92	7318	23	8.5	2	...
4655.....	12 57 47.93	+27 43 35.8	18.05	1.91	20907	34	4.2	2	...
4656.....	12 57 47.86	+27 46 09.7	17.62	1.82	5809	12	12.6	2	...
4659.....	12 57 47.57	+27 50 52.1	19.80	2.06	53361	47	2.0	2	...
4679.....	12 57 46.14	+27 45 25.2	16.13	1.91	6141	15	11.1	2	1
4692.....	12 57 45.74	+27 25 45.6	17.37	1.74	8346	22	7.1	2	...
4703.....	12 57 44.98	+27 09 19.3	19.68	1.60	7191	42	1.9	1	...
4714.....	12 57 43.21	+27 34 39.2	17.54	1.75	7209	12	15.3	2	...
4719.....	12 57 42.84	+27 37 16.6	17.76	2.15	20387	19	12.1	2	...
4749.....	12 57 40.15	+27 32 27.6	19.17	1.72	7206	30	3.7	2	...
4757.....	12 57 39.40	+27 36 22.0	18.46	2.26	21011	27	8.5	2	...
4766.....	12 57 38.10	+27 44 56.3	17.69	1.59	25731	32	4.2	2	...
4768.....	12 57 38.73	+27 27 18.4	19.03	1.66	7588	32	3.2	2	...
4774.....	12 57 37.20	+28 02 25.1	18.14	1.65	6414	44	2.5	1	...
4780.....	12 57 37.11	+27 38 03.9	18.75	2.08	20808	22	7.4	2	...
4788.....	12 57 36.99	+27 09 18.1	17.70	1.92	20826	27	6.3	2	...
4800.....	12 57 36.02	+27 20 23.4	18.30	1.31	25390	89	1.6	1	...
4815.....	12 57 34.68	+27 18 37.1	18.33	2.36	7442	27	6.9	2	...
4825.....	12 57 33.25	+27 29 47.3	19.34	1.63	20988	31	...	9	4
4846.....	12 57 31.51	+27 26 03.4	18.83	2.21	38073	31	5.5	2	...
4851.....	12 57 31.01	+27 25 03.2	20.00	1.59	31987	44	2.5	1	...
4852.....	12 57 30.58	+27 32 34.9	18.36	1.97	7648	13	12.9	2	...
4858.....	12 57 30.37	+27 28 09.2	18.78	2.10	38167	44	4.1	2	...
4871.....	12 57 28.32	+27 58 30.8	18.88	1.30	11148	22	...	9	4
4888.....	12 57 27.51	+27 38 10.3	18.18	1.78	8042	23	5.9	2	...
4891.....	12 57 27.56	+27 26 13.0	19.56	2.51	38113	44	4.3	2	...
4905.....	12 57 26.14	+27 39 33.6	18.20	1.82	5095	36	2.1	2	...
4926.....	12 57 24.69	+27 21 18.6	17.45	2.37	20561	19	11.6	2	...
4928.....	12 57 24.41	+27 29 54.3	13.51	...	7317	20	13.8	2	...
4933.....	12 57 23.47	+27 45 58.5	16.35	1.90	9132	10	16.8	2	...
4937.....	12 57 23.55	+27 32 59.7	18.35	1.82	6039	33	3.9	2	...
4943.....	12 57 22.68	+27 29 34.9	15.88	1.83	8214	32	5.8	2	...
4945.....	12 57 21.73	+27 52 49.3	16.64	1.78	7441	14	11.9	2	...
4967.....	12 57 19.59	+27 36 49.2	18.09	1.67	7776	33	5.1	2	...
4972.....	12 57 18.26	+27 44 50.3	18.07	1.79	7074	48	3.2	2	...
4974.....	12 57 17.80	+27 48 39.2	16.49	1.62	7115	17	9.2	2	...
4987.....	12 57 16.79	+27 37 06.2	16.71	1.93	7257	12	18.0	2	...
5012.....	12 57 14.06	+27 15 13.3	18.43	1.88	5203	38	3.5	2	...
5032.....	12 57 11.96	+27 06 12.2	17.55	1.84	7272	29	5.4	2	...
5038.....	12 57 10.75	+27 24 17.6	16.14	1.82	6215	12	13.6	2	2
5076.....	12 57 07.66	+27 20 25.4	18.73	1.92	7288	29	5.0	2	...
5077.....	12 57 07.78	+27 14 17.6	19.95	2.08	20573	42	3.9	2	...
5094.....	12 57 05.89	+27 16 47.8	19.91	2.44	61388	188	2.4	1	...
5095.....	12 57 04.89	+27 40 38.4	18.74	1.83	7924	63	2.6	1	...

TABLE 1—*Continued*

GMP	(J2000) α	(J2000) δ	b	$b-r$	cz	δcz	R	Q	E
5096.....	12 57 04.56	+27 46 22.5	16.89	1.78	7597	30	5.9	2	...
5100.....	12 57 04.23	+27 43 48.1	17.15	1.71	8881	27	4.8	2	...
5102.....	12 57 04.33	+27 31 33.0	17.50	1.92	8328	20	7.4	2	...
5120.....	12 57 02.59	+27 39 23.7	18.17	1.89	6788	36	5.4	2	...
5155.....	12 56 59.94	+27 20 00.9	19.77	2.65	73400	70	2.7	1	...
5178.....	12 56 55.93	+27 27 44.3	18.61	1.92	7627	32	5.3	2	...
5206.....	12 56 52.62	+27 11 02.9	19.25	2.53	60175	60	3.8	2	...
5217.....	12 56 50.80	+27 37 40.0	18.45	1.78	8113	35	4.7	2	...
5242.....	12 56 48.66	+27 12 13.4	19.37	1.24	25539	35	...	9	3
5250.....	12 56 47.77	+27 25 15.3	16.97	1.83	7762	11	13.9	2	...
5254.....	12 56 47.39	+27 17 31.7	17.71	1.79	7787	25	5.2	2	...
5284.....	12 56 42.37	+27 32 53.3	17.98	1.75	7573	22	6.5	2	...
5296.....	12 56 40.94	+27 26 51.5	18.90	1.83	7321	24	7.3	2	...
5320.....	12 56 38.45	+27 34 15.1	18.80	1.81	7596	22	5.9	2	...
5364.....	12 56 34.20	+27 32 19.7	15.96	2.01	7105	9	23.3	2	...
5402.....	12 56 29.79	+27 45 39.5	19.61	1.88	46090	72	...	9	3
5434.....	12 56 26.29	+27 43 37.9	16.82	1.94	6836	12	16.4	2	...
5455.....	12 56 24.47	+27 32 18.3	19.58	1.73	40921	47	2.2	1	...
5546.....	12 56 14.63	+27 30 22.4	17.42	1.93	7451	14	12.1	2	...
5607.....	12 56 10.21	+27 21 49.2	19.77	2.61	69072	62	2.0	2	...
5673.....	12 56 04.21	+27 17 07.7	18.54	1.57	5800	10	...	9	2
5681.....	12 56 01.93	+27 39 52.2	18.72	1.60	6148	59	2.3	1	...
5713.....	12 56 00.18	+27 14 08.3	19.57	2.07	51105	52	1.4	2	...
5738.....	12 55 56.81	+27 36 51.1	19.74	0.98	27463	44	...	9	4
5909.....	12 55 37.56	+27 20 28.9	19.66	1.93	6332	41	2.2	1	...

ation for these galaxies are $\overline{cz} = 6917 \pm 47$ km s^{-1} (i.e., $\bar{z} = 0.02307 \pm 0.00016$) and $\sigma_{cz} = 1038 \pm 60$ km s^{-1}. The line-of-sight velocity dispersion of the cluster is $\sigma_v = \sigma_{cz}/(1+z) = 1015 \pm 59$ km s^{-1}. In calculating the dispersion and the 1 σ errors for the mean and dispersion we allow for the fact that the standard deviation of a 3 σ clipped Gaussian is 0.983 times the true standard deviation; we also assume a typical error in cz of 50 km s^{-1} and calculate the errors on $\overline{cz}$ and σ_v according to Danese, De Zotti, & di Tullio (1980).

A range of statistical tests confirm the eye's impression (see Fig. 5) that the velocity distribution departs significantly from a Gaussian. A χ^2-test on the data binned as in Figure 5 gives $\chi^2 = 52.8$ with 26 degrees of freedom and rejects a Gaussian at the 99.8% confidence level; the Lilliefors test (the Kolmogorov-Smirnov test accounting for the fact that the mean and dispersion are estimated from the data) rejects a Gaussian at the 99.6% level; the Shapiro-Wilk W-test rejects a Gaussian at the 99.7% level. These departures from Gaussian form cannot, however, be simply characterized in terms of the low-order moments of the distribution: neither the skewness nor the kurtosis is very significantly non-Gaussian.

A much better match to the observed velocity distribution can be achieved with a double Gaussian. A χ^2 fit gives $\overline{cz}_1 = 6539 \pm 146$ km s^{-1}, $\sigma_1 = 1096 \pm 74$ km s^{-1} and $\overline{cz}_2 = 7477 \pm 89$ km s^{-1}, $\sigma_2 = 476 \pm 93$ km s^{-1} with $\chi^2 = 20.9$ for 21 degrees of freedom. The greatly improved fit with a double Gaussian is the first clear suggestion that we are detecting substructure in the line-of-sight velocity distribution.

3.2. *Localized Velocity Structure*

Given the non-Gaussian nature of the velocity distribution and the second peak in the X-ray map around NGC 4839, we clearly should search for spatially localized variations in the line-of-sight velocity distribution. One test that has been commonly used for this purpose is the Δ-test developed by Dressler & Shectman (1988). For each galaxy in the cluster they use the sample of 11 nearest neighbors (including the galaxy itself) to compute a local mean velocity $\bar{v}_{\rm local}$ and velocity dispersion $\sigma_{\rm local}$. They next compute the deviation δ of these values from the mean velocity $\bar{v}$ and dispersion σ for the cluster as a whole using

$$\delta^2 = (11/\sigma^2)[(\bar{v}_{\rm local} - \bar{v})^2 + (\sigma_{\rm local} - \sigma)^2] \,. \quad (1)$$

The test statistic Δ is then the sum of the δ's over the N galaxies in the cluster. Dressler and Shectman choose not to add the δ's in quadrature in order not to overemphasize the largest deviations. For a Gaussian velocity distribution without local variations the expectation value of the statistic is $\langle\Delta\rangle = N$. The expected distribution of the statistic in the absence of localized deviations can, however, be estimated for any given cluster without this assumption by computing Δ for a large number of simulated clusters in which the galaxies have the same positions but have had their velocities randomly reassigned. Dressler and Shectman used this statistic to look for substructure in a set of 15 clusters including Coma. Their test gave no evidence for substructure in Coma, but they used only 100 galaxies, of which only three were in the region of NGC 4839.

It is worthwhile to consider the nature of the Dressler and Shectman test before proceeding further. In essence it breaks down into three parts: (1) a recipe for defining what is "local"; (2) the comparison of one one-dimensional distribution with another, its hypothetical parent; and (3) a recipe for combining all the local comparisons to recover a single statistic for the whole cluster. The first point worth noting is that the statistic δ they adopt for performing part (2) is not what one would a priori choose to compare two one-dimensional distributions, especially if they are not necessarily Gaussian. The usual choices for this task are the χ^2 or K-S D statistics, which are more general (they apply to distributions that cannot be characterized by just the first two moments), more powerful (they are statistically more efficient, able to discriminate different distributions on the basis of smaller samples), and more robust (less susceptible to outliers and pathological cases). Secondly,

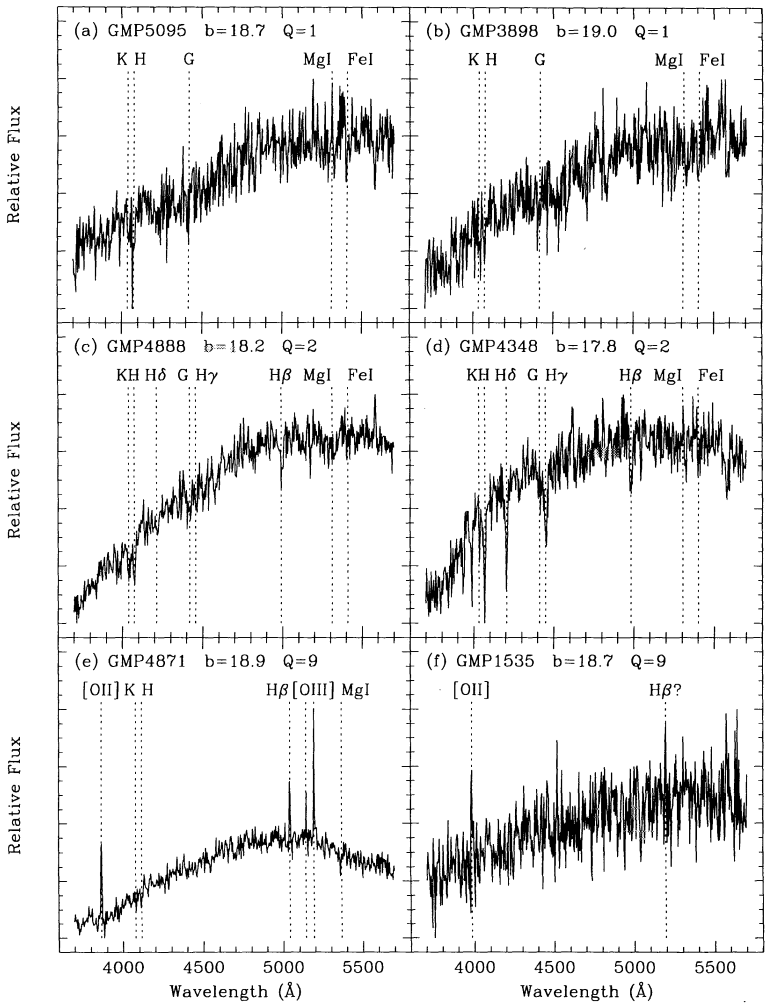

FIG. 3.—Examples of spectra of quality classes $Q = 1$, 2, and 9 with identified features marked: (*a*) GMP 5095, $b = 18.74$, $cz = 7924$ km s^{-1}, $R = 2.6$, $Q = 1$; (*b*) GMP 3898, $b = 19.04$, $cz = 7864$ km s^{-1}, $R = 2.4$, $Q = 1$; (*c*) GMP 4888, $b = 18.18$, $cz = 8042$ km s^{-1}, $R = 5.9$, $Q = 2$; (*d*) GMP 4348, $b = 17.77$, $cz = 7576$ km s^{-1}, $R = 2.2$, $Q = 2$; (*e*) GMP 4871, $b = 18.88$, $cz = 11{,}148$ km s^{-1}, $Q = 9$, $E = 4$; (*f*) GMP 1535, $b = 18.71$, $cz = 21{,}222$ km s^{-1}, $Q = 9$, $E = 1$.

the scale imposed by the choice of the 11 nearest neighbors may not be the scale on which substructure is most obvious—clearly it is of interest to examine such statistics over a range of scales by allowing the number of nearest neighbors to vary. Finally, it would be helpful to have a statistic that was readily interpreted.

With these considerations in mind, we have devised a new test, in the spirit of the Dressler-Shectman test, for detecting localized variations in the velocity distribution. For each galaxy we compare the velocity distribution of the n nearest neighbors to the velocity distribution of the whole cluster via a standard K-S two-sample test (see, e.g., Press et al. 1986, pp. 472–475). We define our test statistic κ_n to be

$$\kappa_n = \sum_{i=1}^{N} -\log\left[P_{\rm KS}(D > D_{\rm obs})\right], \qquad (2)$$

where the sum is over the N galaxies in the cluster and $P_{\rm KS}(D > D_{\rm obs})$ is the probability of the K-S statistic D being greater than the observed value $D_{\rm obs}$, which can be straightforwardly computed (see Press et al.). κ_n is thus just the (negative) log-likelihood that there is no localized deviation in the velocity distribution on the scale of groups of n nearest neighbors—the larger κ_n, the greater the likelihood that the local velocity distribution is different from the overall distribution. As with the Dressler-Shectman statistic, the significance of κ_n can be straightforwardly estimated by Monte Carlo simulations in which the velocities of the cluster galaxies are shuffled randomly.

Table 2 gives the results of applying this test to our catalog of redshifts in Coma. For various group sizes n, it gives the probability that κ_n is greater than the observed value $\kappa_n^{\rm obs}$ and the number of simulations used to determine this probability. It is clear that the velocity distribution in the Coma cluster has

TABLE 2

RESULTS OF κ-TEST

n	$P(\kappa_n > \kappa_n^{\rm obs})$	Simulations
2	0.018	1×10^3
10	0.0003	3×10^4
20	0.0009	3×10^4
50	0.0015	4×10^4
100	0.0050	3×10^4
200	0.015	1×10^3

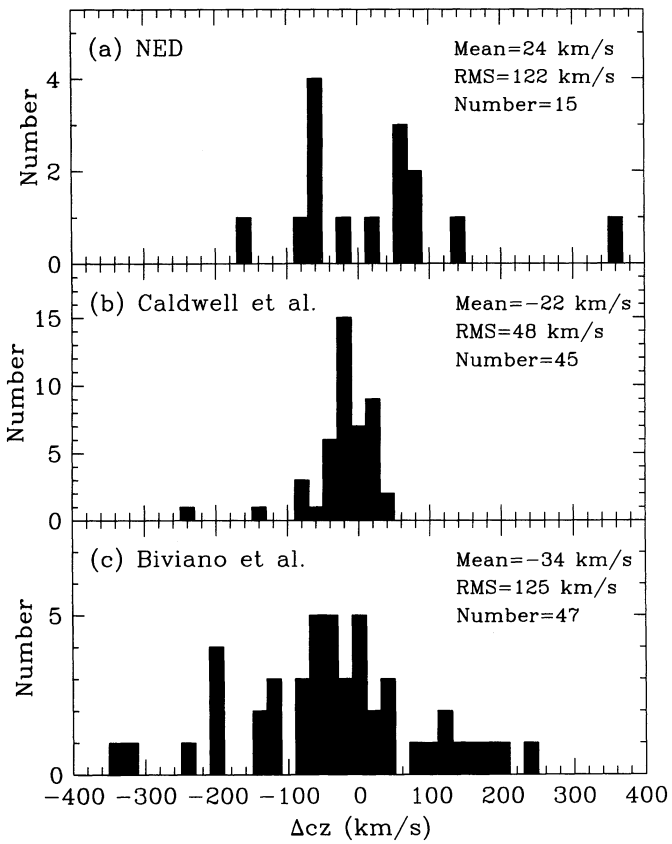

FIG. 4.—Distribution of the differences in *cz* between the measurements reported here and literature values for (*a*) 15 galaxies with redshifts in NED, (*b*) 45 galaxies with redshifts by Caldwell et al. (1993), and (*c*) 47 galaxies with redshifts by Biviano et al. (1995).

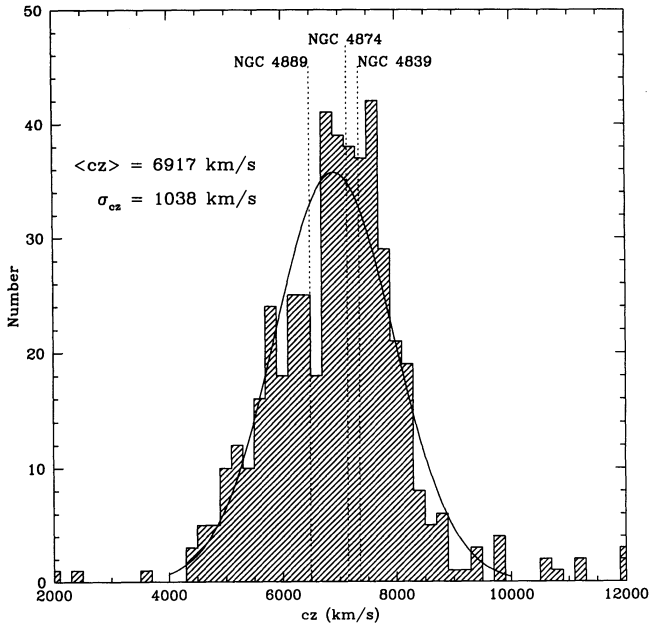

FIG. 5.—Distribution of radial velocities for galaxies in the Coma cluster. The curve is a Gaussian with mean 6917 km s^{-1} and standard deviation 1038 km s^{-1}. The velocities of the three dominant cluster galaxies are indicated.

highly significant local variations for subgroups of galaxies with a broad range of sizes. The *location* of this localized variation is shown using groups of size $n = 10$ and 50 in the bubble plots of Figures 6 and 7. In these plots the size of the bubble at the position of each galaxy is proportional to $-\log [P_{KS}(D > D_{obs})]$, so that larger bubbles indicate a larger difference between the velocity distribution of the n nearest neighbors and the overall cluster velocity distribution. There are two clusters of large bubbles indicating two subclusters with differing velocity distributions. One is centered on the main body of the cluster, and the other is centered around NGC 4839.

Figure 8 shows the velocity distributions in different regions of the cluster suggested by the above result: (*a*) within 20′ of the cluster center; (*b*) outside 20′ of the center; (*c*) within 20′ of NGC 4839; and (*d*) further than 20′ from both the cluster center and NGC 4839. The velocities of the three dominant cluster galaxies are indicated. For each of these four regions Table 3 gives the confidence level at which the skewness, K-S, and *W* tests reject a Gaussian distribution, together with the probability that each sample's velocity distribution is consistent with that of the sample within 20′ of the cluster center under a two-sample K-S test. As the figure shows, and the table confirms quantitatively, the deviation of the overall velocity distribution from a Gaussian can be almost entirely explained as being due to a subcluster centered on NGC 4839.

A skewness in the velocity distribution outside the cluster core was first noted by Merritt (1987). Merritt & Gebhardt (1996) showed that this skewness was confined to distances between 16′ and 40′ from the cluster center, but did not identify it with the NGC 4839 subcluster. Once the region around NGC 4839 is excluded the skewness disappears, and the velocity distribution in the outer regions is found to be statistically consistent with that in the cluster core (Fig. 8 and Table 3; see Fig. 5 of Merritt & Gebhardt 1996).

3.3. *Characterization of Subclusters*

Having shown the existence of localized variations in the line-of-sight velocity distribution, and established that these are due to the galaxies around NGC 4839, we now attempt to characterize the membership and properties of the main cluster and the NGC 4839 subcluster.

TABLE 3

LOCAL VELOCITY DISTRIBUTIONS

SAMPLE REGION	*N*	CONFIDENCE LEVELS			$P_{KS}(n\|1)$
		Skew	K-S	*W*	
1. <20′ from center	188	70%	75%	90%	...
2. >20′ from center	277	99.3	99	99.9	0.15
3. <20′ from NGC 4839	81	98.4	99	99.9	0.03
4. >20′ from both center and NGC 4839	196	92	95	98	0.32

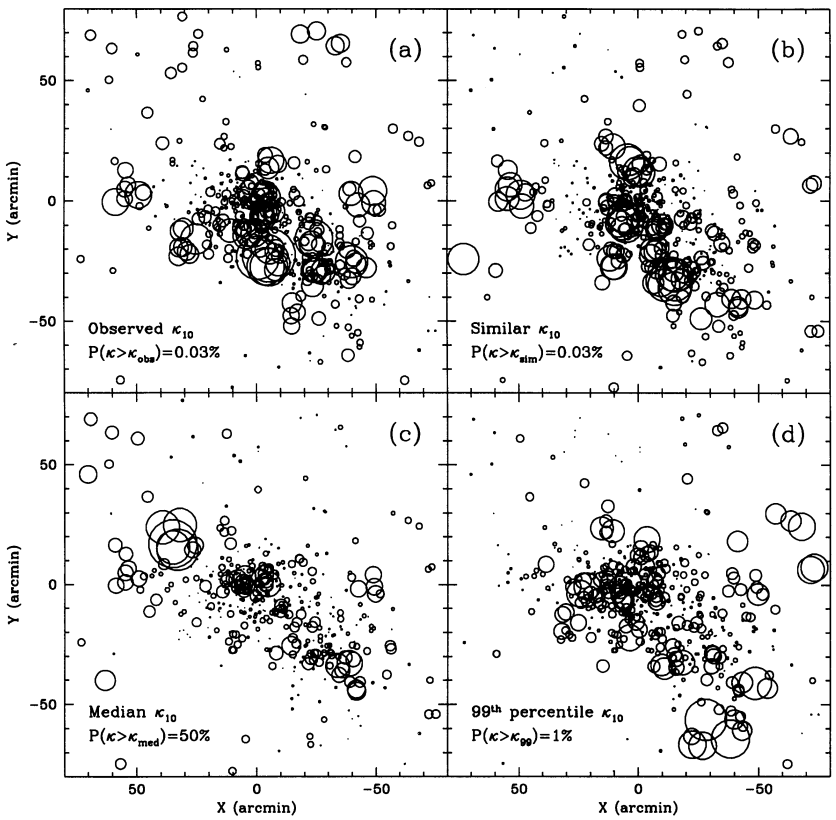

FIG. 6.—Bubble plots showing the degree of difference between the local velocity distribution for groups of 10 nearest neighbors compared to the overall velocity distribution. The size of the bubble at the position of each galaxy is proportional to the log-likelihood of the local and overall distributions *not* being the same under a K-S two-sample test. Panel (*a*) shows the observed distribution, with the largest bubbles concentrated around the cluster core and the NGC 4839 cluster; panel (*b*) shows the simulation with κ most similar to the observed value; panel (*c*) shows the simulation with the median value of κ; panel (*d*) shows the simulation with the 99th percentile value of κ.

A powerful tool for this task is the KMM mixture-modeling algorithm (McLachlan & Basford 1988), recently introduced to the study of galaxy clusters by Bird (1994). This algorithm attempts to find the maximum-likelihood partition of a data set into a specified number M of N-dimensional subclusters (see Ashman & Bird 1994). The M subclusters are each assumed to have N-dimensional Gaussian distributions, with possibly different scale lengths in each dimension. The algorithm returns an estimate of the confidence level at which the M-cluster hypothesis is preferred to the null hypothesis of a single cluster, as well as the partition of the objects into M Gaussian subclusters and the location and scale of each subcluster. The limitations of this algorithm are (1) the lack of a decisive way to determine the optimum number of subclusters and (2) the necessary assumption that the subclusters are N-dimensional Gaussians. The former limitation is met by simply adopting the smallest number of subclusters that provides an adequate representation of the data. The latter is not too limiting for the study of clusters of galaxies, since each subcluster is supposed to be virialized and so have a Gaussian velocity distribution and a projected spatial distribution that is at least qualitatively similar to a Gaussian.

We here apply the KMM algorithm in three dimensions: the projected positions of the galaxies on the sky and the line-of-sight velocities. We use the 436 galaxies with $4000 < cz < 10{,}000$ km s^{-1} lying within 70′ of the cluster center. We concentrate on a partition into just two groups, as this turns out to be optimum. The algorithm can start iterating toward the maximum-likelihood solution from either an initial partition of the sample into groups or from a set of initial parameters for each group. Table 4 lists the various initial parameters/partitions that we used and the corresponding final solutions the algorithm arrived at: $\langle x_1, y_1, v_1\rangle$ and $\langle x_2, y_2, v_2\rangle$ are the mean positions and velocities of the two subclusters, $\sigma(x_1, y_1, v_1)$ and $\sigma(x_2, y_2, v_2)$ are the standard deviations in these coordinates, and f_1 and f_2 are the fractions of the sample in the two subclusters. The table also gives the KMM algorithm's estimate of the overall rate for the correct allocation of objects to groups.

Given our previous results, we first look for a partition into two groups corresponding to the main body of Coma and the subcluster around NGC 4839. In case 1 we chose to specify initial positions and dispersions for the two subclusters (see Table 4), while in case 2 we specified a partition of the sample in which the NGC 4839 subcluster was taken to be all galaxies within $R = 20'$ and $\Delta v = \pm 1200$ km s^{-1} of NGC 4839. Although specified differently, the starting parameters for these two cases are quite similar and the final solutions reached were identical (i.e., an identical final partition into subclusters). The two-group solution was strongly favored compared to the one-group solution and the estimate of the correct allocation rate was 96%.

The critical question is how robust this final partition is under changes in the initial parameters. Cases 3–7 show that even initial guesses quite far from this solution converge to very similar results. In cases 3–5 the subclusters are defined as

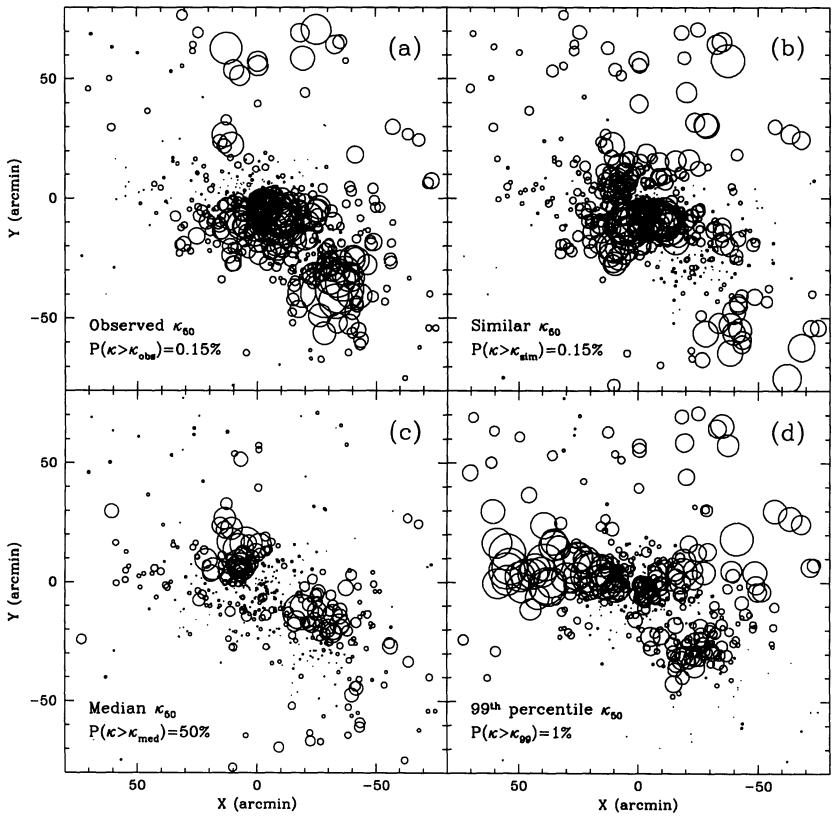

FIG. 7.—Same as Fig. 6 but for groups of 50 nearest neighbors

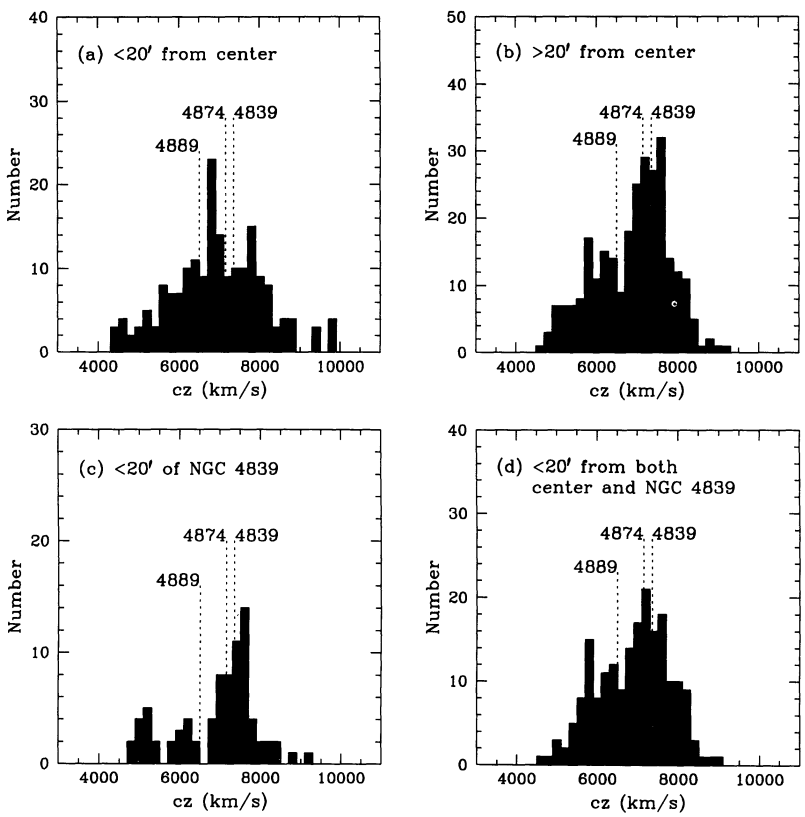

FIG. 8.—Velocity distributions for cluster galaxies (*a*) within 20′ of the cluster center; (*b*) outside 20′ of the center; (*c*) within 20′ of NGC 4839; and (*d*) further than 20′ from both the cluster center and NGC 4839. The velocities of the three dominant cluster galaxies are indicated.

TABLE 4

RESULTS FROM KMM ALGORITHM

Case	$\langle x_1, y_1, v_1 \rangle$	$\sigma(x_1, y_1, v_1)$	$\langle x_2, y_2, v_2 \rangle$	$\sigma(x_2, y_2, v_2)$	(f_1, f_2)	Rate (%)
			Initial Parameters			
1.....	(0.0, 0.0, 6800)	(30, 30, 1100)	(−30.0, −30.0, 7400)	(20, 20, 400)	(0.85, 0.15)	...
2.....	(−0.8, −3.4, 6840)	(23, 20, 1082)	(−29.3, −26.9, 7356)	(9, 8, 456)	(0.87, 0.13)	...
3.....	(−2.2, −4.6, 6857)	(23, 20, 1064)	(−29.9, −27.3, 7460)	(7, 6, 336)	(0.91, 0.09)	...
4.....	(1.3, −1.8, 6821)	(23, 20, 1102)	(−27.4, −24.9, 7250)	(11, 11, 620)	(0.79, 0.21)	...
5.....	(6.2, 2.2, 6930)	(20, 18, 1059)	(−26.0, −24.0, 6870)	(13, 13, 990)	(0.66, 0.34)	...
6.....	(0.0, 0.0, 7400)	(20, 20, 1000)	(−30.0, −30.0, 6800)	(10, 10, 999)	(0.50, 0.50)	...
7.....	(0.0, 0.0, 7000)	(20, 20, 1000)	(−30.0, −30.0, 7000)	(10, 10, 999)	(0.50, 0.50)	...
8.....	(1.0, 1.0, 7000)	(20, 20, 1000)	(−1.0, −1.0, 7000)	(20, 20, 999)	(0.50, 0.50)	...
			Final Parameters			
1.....	(−0.9, −3.6, 6853)	(22, 19, 1082)	(−33.1, −29.0, 7339)	(12, 14, 329)	(0.87, 0.13)	96
2.....	(−0.9, −3.6, 6853)	(22, 19, 1082)	(−33.1, −29.0, 7339)	(12, 14, 329)	(0.87, 0.13)	96
3.....	(−0.9, −3.6, 6853)	(22, 19, 1082)	(−33.1, −29.0, 7339)	(12, 14, 329)	(0.87, 0.13)	96
4.....	(−0.9, −3.6, 6853)	(22, 19, 1082)	(−33.1, −29.0, 7339)	(12, 14, 329)	(0.87, 0.13)	96
5.....	(−0.1, −3.4, 6841)	(22, 19, 1086)	(−34.1, −27.3, 7353)	(13, 18, 354)	(0.85, 0.15)	95
6.....	(−0.1, −3.4, 6841)	(22, 19, 1086)	(−34.1, −27.3, 7353)	(13, 18, 354)	(0.85, 0.15)	95
7.....	(−0.1, −3.4, 6841)	(22, 19, 1086)	(−34.1, −27.3, 7353)	(13, 18, 354)	(0.85, 0.15)	95
8.....	(−0.9, −7.2, 6788)	(23, 14, 1119)	(−15.2, −5.0, 7256)	(24, 32, 625)	(0.84, 0.16)	83

in case 2 but with the NGC 4839 subcluster having $R = 15'$, $25'$, $30'$, $\Delta v = \pm 900$, 1500, 2000 km s^{-1} and a fraction of galaxies $f_2 = 0.09$, 0.21, 0.34, respectively. Cases 3 and 4 converge to the exact same result as cases 1 and 2, while case 5 converges to a very similar result (the change is due to six galaxies being reallocated from the main cluster to the NGC 4839 subcluster). The initial parameters in cases 6 and 7 differ more radically from the best solution. In case 6 the positions and sizes are set to sensible values, but the mean velocities are reversed, the velocity dispersions for both subclusters are set to 1000 km s^{-1}, and the fraction of galaxies in each is set to 0.5. Case 7 is the same as case 6 but this time both clusters have their mean velocity set to 7000 km s^{-1}—this set of initial parameters corresponds to using the projected distribution to separate the subclusters while making no assumptions about their velocity distributions. Even these two cases, with quite incorrect initial parameters, converge to the same solution as case 5. Only if we throw away the information on subclustering from the velocity distribution *and* the projected positions of the galaxies do we fail to achieve a similar solution. In case 8 we make the initial parameters for the two subclusters identical apart from a trivial symmetry-breaking difference in their positions. We then get a quite different result, with two oddly placed and more elliptical subclusters and a significantly lower correct allocation rate.

The partition into two subclusters (the main Coma cluster and the NGC 4839 group) would therefore appear to be very robust. Figure 9 shows the final partition of the sample on the sky and in line-of-sight velocity corresponding to the solution for cases 1–4. It is instructive to compare the positions and velocities of the two subclusters, at (−0.9, −3.6, 6853) and (−33.1, −29.0, 7339), with those of the three dominant galaxies in the cluster: NGC 4874 at (−1.6, −0.7, 7152), NGC 4889 at (5.6, 0.4, 6494), and NGC 4839 at (−30.7, −28.3, 7352). The center of the main subcluster lies just 3.0 from NGC 4874, while the center of the secondary subcluster lies just 2.5 from NGC 4839. The mean velocity of the secondary subcluster is identical (within the measurement errors) to the velocity of NGC 4839. However, NGC 4874 and NGC 4889 lie +299 km s^{-1} and −359 km s^{-1}, respectively, from the mean velocity of

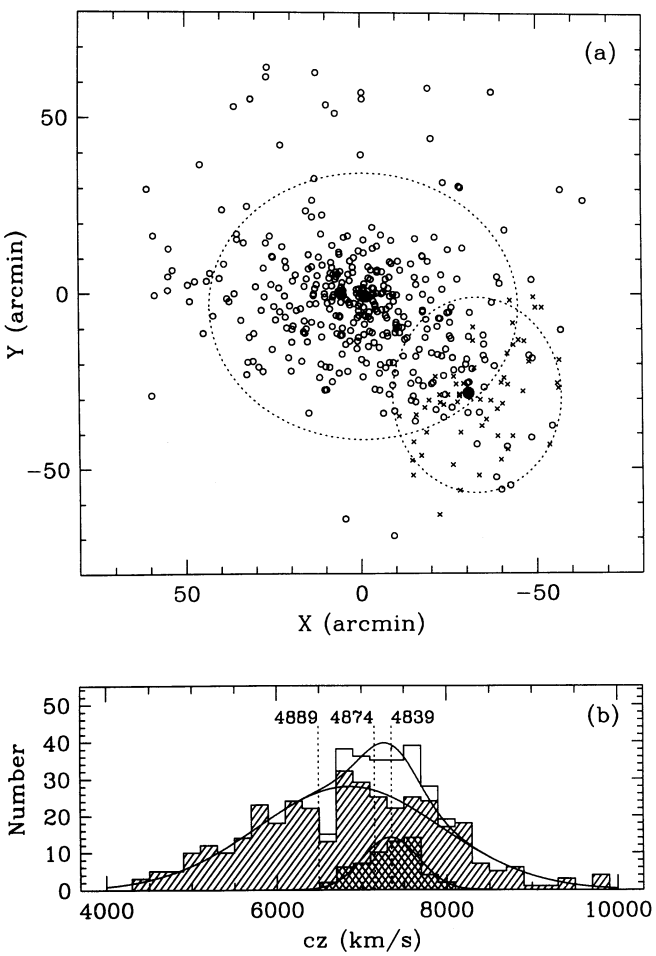

FIG. 9.—Partition into two subclusters by the KMM algorithm. (*a*) The projected positions, with galaxies in the main cluster shown as circles and those in the NGC 4839 subcluster as crosses. The filled circles are the three dominant galaxies. The dotted ellipses are the 2 σ contours of the fitted Gaussians. (*b*) The velocity distributions for the entire data set, the main cluster, and the NGC 4839 subcluster, with the fitted Gaussians overlaid.

the main cluster (to which they clearly belong). Since the standard error in this mean is 111 km s^{-1}, their peculiar velocities are statistically significant.

If we apply the same Gaussianity tests to these subclusters that we applied to the cluster as a whole, we find little evidence for non-Gaussian velocity distributions. The only statistic significant at more than 90% confidence is the W-test when applied to the main subcluster, which would appear to be picking up the deficit of galaxies with velocities around 6600 km s^{-1} that can be seen in Figure 9. In general, however, the velocity distribution in Coma is well fitted by two Gaussians and there is no evidence for further significant subclustering.

The velocity parameters determined by this analysis give an accurate picture of the velocity structure in the cluster, since no observational biases were imposed on the measured redshifts. However, the relative numbers of galaxies in the two subclusters and (to a lesser extent) the projected sizes are affected by the particular regions in which we chose to obtain redshifts (see Fig. 1). We, therefore, do not obtain a reliable estimate of the relative richness of the subclusters from this analysis.

An alternative visualization of the subclustering is provided by Figure 10, which shows the smoothed density of galaxies as a function of velocity and distance from the cluster center along the NE–SW diagonal [i.e., $(X + Y)/2^{1/2}$, with NE positive]. The latter coordinate was chosen so as to maximize the separation of the main cluster and the NGC 4839 subcluster. The smoothing was obtained with a two-dimensional Gaussian kernel with a spatial dispersion of 8′ and a velocity dispersion of 300 km s^{-1}. These values were guided by physical scales in the cluster rather than by statistical considerations: 8′ is approximately the cluster core radius, while 300 km s^{-1} is about the scale of the smallest velocity dispersions of groups of galaxies. The positions of the three dominant galaxies are indicated. The NGC 4839 group (with NGC 4839 close to its center) stands out clearly in the spatial coordinate but not in velocity (as Fig. 9*b* implies). However, this figure also shows interesting structure in the cluster core.

3.4. *Core Structure*

Figure 10 shows a correlation between position and velocity in the core of the main Coma cluster, with lower velocities to the SE and higher velocities to the NW. Given the finding of Fitchett & Webster (1987) that there is double structure in the projected galaxy distribution in the core of Coma centered on NGC 4874 and NGC 4889, it is no surprise to see that these two dominant galaxies are projected in the spatial dimension onto the primary and secondary peaks, respectively, in the core galaxy distribution. Contrary to naive expectation, however,

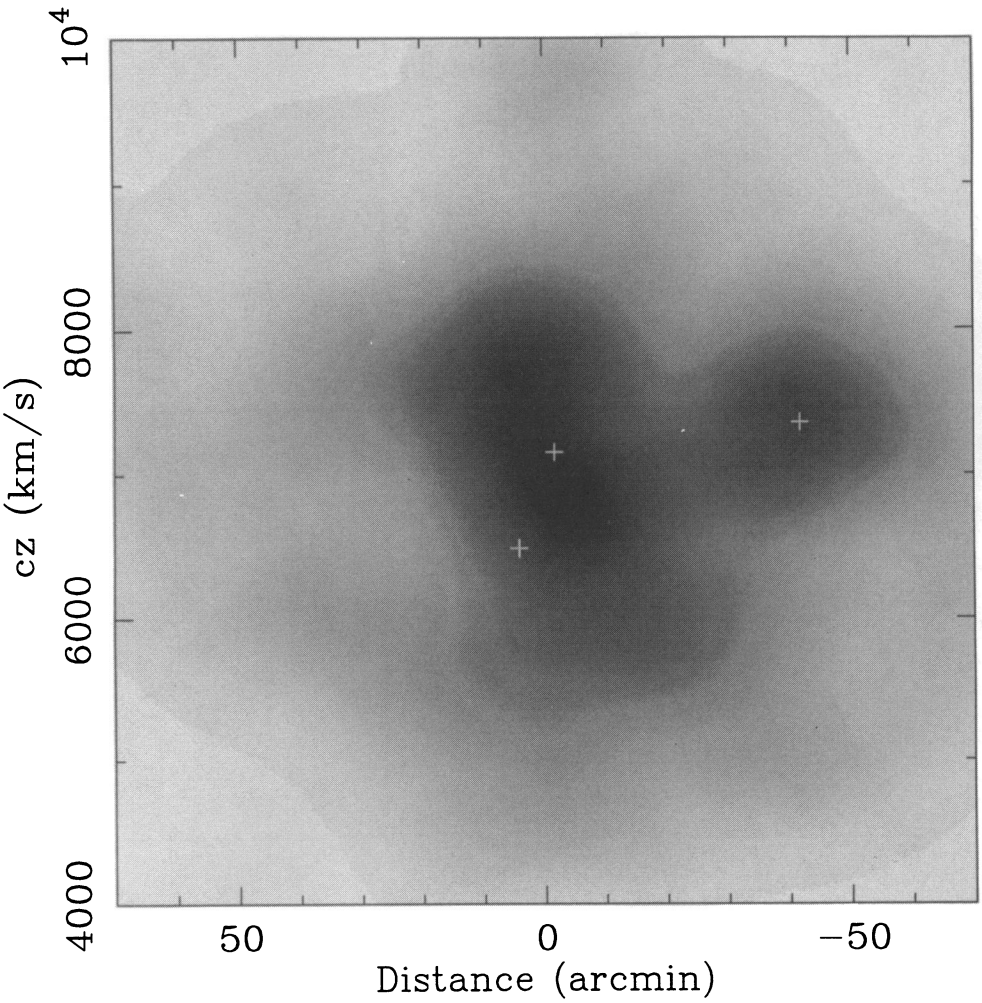

FIG. 10.—Galaxy density distribution projected onto the plane of radial velocity versus projected distance from the cluster center along the NE–SW diagonal (NE positive). The density is smoothed with a Gaussian of dispersion 8′ in the spatial dimension and 300 km s^{-1} in the velocity dimension. The positions of the three dominant galaxies are marked by crosses (*left to right*: NGC 4889, NGC 4874, NGC 4839). The gray scale is linear with density and runs from zero to the maximum.

their velocities are *not* well matched to the mean velocities of the peaks they are projected onto—NGC 4874 has a velocity about 350 km s^{-1} higher and NGC 4889 has a velocity about 1100 km s^{-1} lower. In fact, the positions of the peaks and the dominant galaxies appear to be almost mirror-symmetric in velocity.

The significance of the correlation between position and velocity can be determined using rank correlation statistics. Taking the galaxies in a 30′ × 30′ central region with 6000 km s^{-1} < cz < 8000 km s^{-1}, we find that the Spearman ρ and Kendall τ statistics imply correlations significant at the 98.5%, 79%, and 99.3% confidence levels for X versus Y, X versus cz, and Y versus cz; for $X + Y$ versus $X - Y$, $X + Y$ versus cz, and $X - Y$ versus cz the correlations are significant at the 63%, 99.5%, and 35% levels. Thus, virtually all the correlation is in $X + Y$ versus cz as shown in Figure 10. This trend is also illustrated in Figure 11, which shows four slices through the $X - Y$–cz galaxy density distribution, smoothed using a three-dimensional Gaussian filter with (σ_X, σ_Y, σ_{cz}) = (8′, 8′, 300 km s^{-1}). In each slice the cluster core dominates, with the NGC 4839 group peaking strongly in the slice at cz = 7250 km s^{-1}. There is also a hint, at a much lower significance level, of a structure about 50′ due east of the cluster center. However, the feature in the figure that is relevant here is the shift in the centroid of the cluster core: at 6500 km s^{-1} the centroid is closer to NGC 4874 (which has cz = 7152 km s^{-1}), at 7250 km s^{-1} it is midway between the two central dominant galaxies, and at 8000 km s^{-1} it is closer to NGC 4889 (which has cz = 6494 km s^{-1}).

Applying the KMM algorithm to the galaxies in the cluster core is somewhat unsatisfactory. If no restriction is imposed on the velocity range the algorithm does not converge to a single well-defined final partition; if attention is limited to velocities in the range 6000 km s^{-1} < cz < 8000 km s^{-1} then two subclusters with centers and mean velocities consistent with Figures 10 and 11 are recovered, but their sizes and velocity

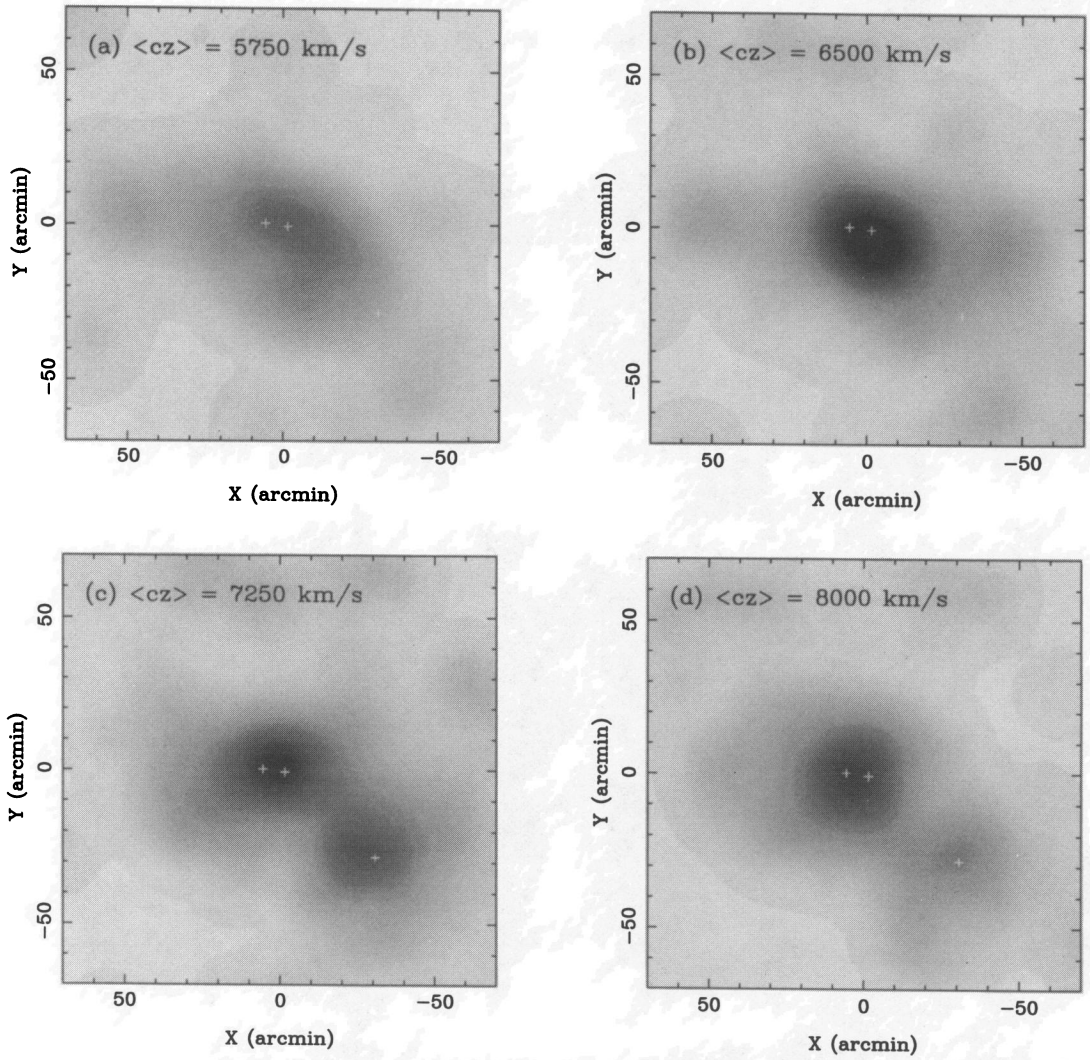

FIG. 11.—Four cuts in velocity through the $X - Y$–cz galaxy density distribution. The density is smoothed with a three-dimensional Gaussian with (σ_X, σ_Y, σ_{cz}) = (8′, 8′, 300 km s^{-1}). The gray scale is linear with density and runs from 0 to the maximum. (*a*) $\overline{cz}$ = 5750 km s^{-1}: This cut shows, at a low level, the cluster core and a clump 50′ to the east. (*b*) $\overline{cz}$ = 6500 km s^{-1}: This cut is near to the peak of the density in cz and also to the velocity of NGC 4889 (6494 km s^{-1}). The projected center of the cluster core is close to the position of NGC 4874. There are low-level structures to the east and west. (*c*) $\overline{cz}$ = 7250 km s^{-1}: This cut is close to the mean velocity of the NGC 4839 group, which shows up strongly. It is also close to the velocity of NGC 4874 (7152 km s^{-1}), although the centroid of the cluster core is now midway between NGC 4874 and NGC 4889. (*d*) $\overline{cz}$ = 8000 km s^{-1}: This cut again shows the NGC 4839 group. The core centroid is now close to NGC 4889, even though the latter's velocity is 1500 km s^{-1} lower.

dispersions reflect mostly the imposed limits. Nonetheless, the two-group solution is strongly favored over the one-group solution, with one subcluster having NGC 4874 close to its projected center and a mean velocity of around 6800 km s^{-1} and the second having NGC 4889 close to its projected center and a mean velocity of around 7600 km s^{-1}.

4. CLUSTER DYNAMICS

4.1. *Field Galaxy Infall*

The kinetic energy K and gravitational potential energy W of field galaxies falling freely onto a cluster are related by $|K/W| \approx 1$, whereas galaxies in a virialized cluster core will have $|K/W| \approx \frac{1}{2}$. Thus, the velocity dispersions of infalling and virialized galaxies are related by $\sigma_{\rm infall} \approx 2^{1/2}\sigma_{\rm virial}$. Huchra (1985) showed that the velocity dispersions of the spirals and elliptical galaxies in the Virgo cluster neatly accorded with this prediction, leading to the identification of the spirals as an infalling field population and the ellipticals as a virialized cluster population.

Lacking morphological classifications for the GMP sample we use the color-magnitude diagram to distinguish early- and late-type galaxies. Figure 12*a* shows the distribution of $b - r$ versus b for the GMP sample, with its clearly defined color-magnitude relation for early-type galaxies. If we compare (Fig. 12*b*) the surface density profiles of the early- and late-type galaxies brighter than $b = 18$ (minimizing the contribution of background objects), we see that (as expected) the early-type galaxies have a significantly steeper profile and dominate in the cluster core, where there is a large relative deficit of late-type galaxies.

The velocity distributions of the early- and late-type galaxies belonging (according to the KMM partition) to the main subcluster are shown in Figure 12*c*. The early types are consistent with the overall velocity distribution of the main subcluster (as they must be, given their dominance), but the late types have a

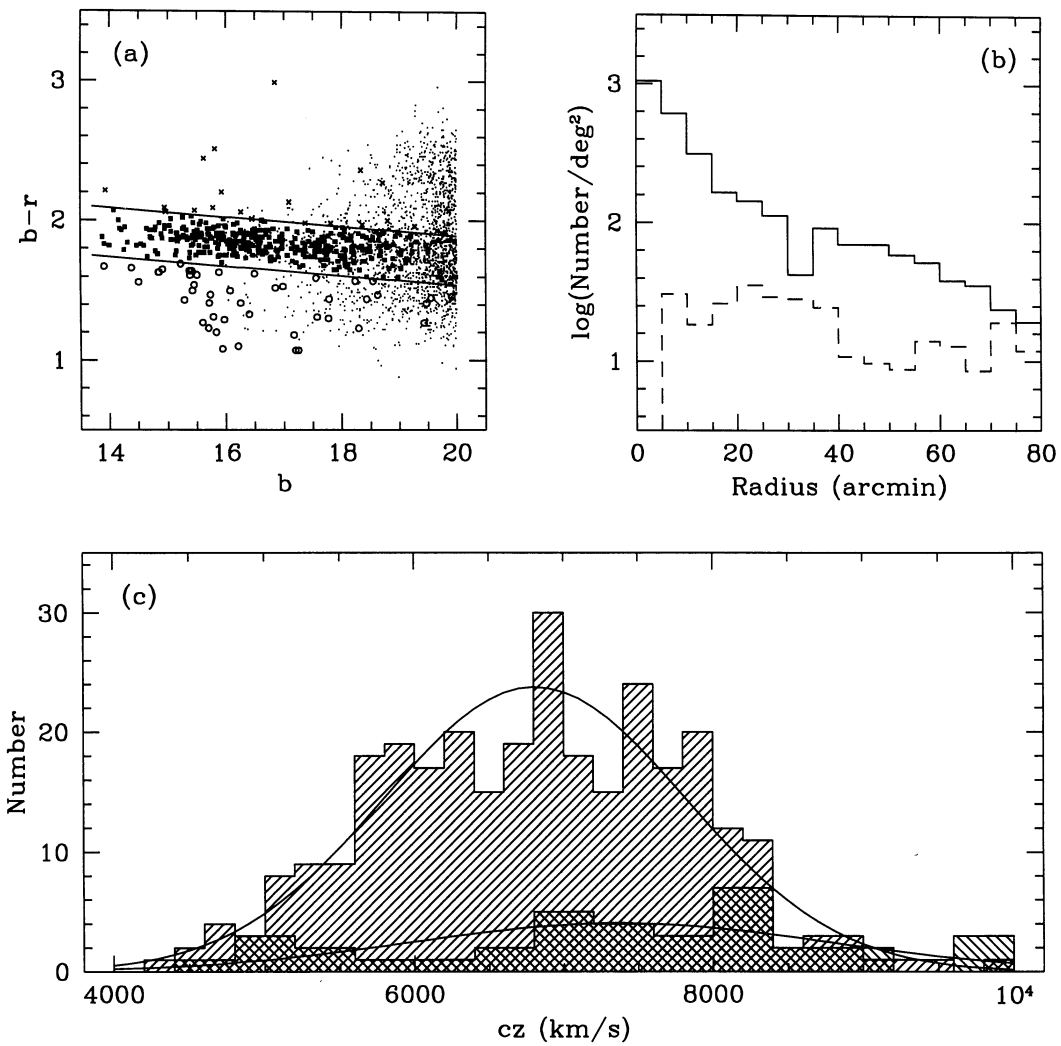

FIG. 12.—(*a*) Color-magnitude diagram for Coma. Small dots are galaxies either without redshifts or with redshifts outside the range 4000–10,000 km s^{-1}; large symbols are for cluster galaxies in this redshift range. These cluster galaxies are shown as squares if they lie between the two lines delimiting the color-magnitude relation for early-type galaxies, as circles if they are bluer than the lower envelope of this relation, and as crosses if they are redder than the red envelope. (*b*) The surface density profiles for the early- and late-type galaxies (respectively, those within and below the color-magnitude relation envelope shown in panel [*a*]) brighter than $b = 18$. The histogram for the early types is solid and the histogram for the late types is dashed. (*c*) The velocity histograms for the 303 early- and 36 late-type galaxies belonging to the main subcluster. The mean redshift and velocity dispersion for the early types are 6807 km s^{-1} and 1017 km s^{-1}, and for late types 7375 km s^{-1} and 1408 km s^{-1}.

velocity dispersion that is approximately $2^{1/2}$ larger and statistically inconsistent with that of the early types—a two-sample KS test shows that the distributions of the two types have only a 0.8% probability of being consistent. A similar analysis applied to the NGC 4839 subcluster finds that the velocity distributions of the early and late types there are consistent with each other, though the samples are much smaller. Although there is some suggestion in Figure 12*c* that some of the late types assigned to the main subcluster might actually belong to the NGC 4839 subcluster, the velocity distributions clearly support the hypothesis that the early types are a virialized population and the late types are still freely falling onto the cluster.

4.2. *Cluster Mass*

The best estimates of the mass of the Coma cluster now come from the X-ray data. Hughes (1989) combined the available X-ray and optical data to derive the mass inside 0.5 h^{-1} Mpc and 2.5 h^{-1} Mpc for a range of models. He found that the preferred models are those in which the mass follows the light, for which the mass inside 0.5 h^{-1} Mpc is $M_{0.5} = 2.6$–$3.4 \times 10^{14}\ h^{-1}\ M_\odot$ and the mass inside 2.5 h^{-1} Mpc is $M_{2.5} = 0.8$–$1.1 \times 10^{15}\ h^{-1}\ M_\odot$. Hughes also determined the minimum and maximum mass profiles consistent with all the data if the mass-to-light ratio of the data was not constrained to be a constant, obtaining allowed mass ranges of $M_{0.5} = 1.9$–$3.6 \times 10^{14}\ h^{-1}\ M_\odot$ and $M_{2.5} = 0.5$–$1.5 \times 10^{15}\ h^{-1}\ M_\odot$.

Briel et al. (1992) used their *ROSAT* survey image to measure the X-ray surface brightness out to 100′ from the cluster center. They find that the binding mass is more centrally concentrated than the X-ray gas, and obtain $M_{2.5} = 0.6$–$1.2 \times 10^{15}\ h^{-1}\ M_\odot$, with a fraction $0.11 \pm 0.05\ h^{-3/2}$ of this mass in hot gas. They reduced the uncertainty in the cluster mass from the factor of 3 given by Hughes to a factor of 2 due to the fact that their X-ray surface brightness profile (derived excluding the region around NGC 4839) reaches twice as far out as any previous measurement and so provides a stronger constraint on the mass profile at large radii. Another mass estimate is given by Watt et al. (1992), who obtained an X-ray image of Coma with a telescope flown on *Spacelab 2*. They give $M_{0.5} = 2.1$–$2.6 \times 10^{14}\ h^{-1}\ M_\odot$ and a best-fitting total mass of $1.3 \times 10^{15}\ h^{-1}\ M_\odot$. Both the Briel et al. and Watt et al. mass estimates are consistent with Hughes's earlier values, and with the masses obtained from the optical galaxy data by Merritt (1987) and The & White (1986). More recent analyses of the galaxy data, which use the line-of-sight velocity distribution to constrain the relative distributions of the dark and luminous matter (Merritt & Saha 1993) or take a nonparametric approach to reconstructing the density profile (Merritt & Gebhardt 1996), also yield similar results, while emphasizing the large uncertainties in determinations of the mass distribution from the galaxy kinematics alone.

Although the X-ray mass determinations remain superior, we can use our expanded sample of galaxy redshifts and our partition of this sample into the main Coma cluster and the NGC 4839 group to obtain improved optical estimates for the total masses of these two components. The virial mass estimator gives $0.9 \times 10^{15}\ h^{-1}\ M_\odot$ for the main cluster and $0.6 \times 10^{14}\ h^{-1}\ M_\odot$ for the NGC 4839 group. Some estimate of the range of allowed masses (assuming mass follows light) is given by using the projected mass estimator (Bahcall & Tremaine 1981; Heisler, Tremaine, & Bahcall 1985) assuming isotropic and linear orbits, which probably under- and overestimate the mass, respectively. For these estimators we find total masses of 0.6–$1.1 \times 10^{15}\ h^{-1}\ M_\odot$ for the main cluster and 0.5–$1.0 \times 10^{14}\ h^{-1}\ M_\odot$ for the NGC 4839 group. These estimates for the mass of the main cluster are in good agreement with all the X-ray estimates. The mass of the NGC 4839 group is 5%–10% of the mass of the main cluster, broadly consistent with the relative numbers of galaxies and the relative X-ray luminosities. Although Hughes (1989) finds that the preferred model is one in which mass follows light, it should be noted that a broader class of models in which the radial profiles of the mass-to-light ratio and the galaxies' orbital anisotropy vary together are also consistent with the data and yield a wider range of mass estimates.

4.3. *Two-Body Models*

The simplest dynamical model for the Coma cluster/NGC 4839 group system is the two-body model of Peebles (1971), first applied to clusters by Beers, Geller, & Huchra (1982) and Gregory & Thompson (1984). In this model the two clusters act as point masses following a linear orbit under their mutual gravity. The clusters are presumed to have started with zero separation and then to have moved apart before turning around and coming together again (the model assumes that the clusters are moving apart or together for the first time). Given the projected separation of the two clusters R_p, their relative radial velocity V_r, and their total mass M, the model yields the projection angle of the system α, the true three-dimensional separation R and relative velocity V, and the mass required to bind the system $M_{\rm bind}$ (note that α is independent of H_0 while the radii and masses scale as h^{-1}). Because of the ambiguity inherent in seeing the system only in projection, the model usually leads to more than one orbital solution, corresponding to various values of α (the angle between the line joining the two clusters and the plane of the sky).

The two-body model neglects any angular momentum the system may have, ignores any matter outside the two subclusters and does not allow for the distribution of matter within the individual clusters (which will become important when they are close to merger). Nonetheless, it provides the best available description for double cluster systems given the limited dynamical constraints. It has previously been applied to a number of double clusters by Colless (1987) and Beers et al. (1991).

The input parameters for a two-body model of the Coma cluster and NGC 4839 group are provided by the KMM analysis (Table 4), which gives $R_p = 0.81 \pm 0.06\ h^{-1}$ Mpc (for $q_0 = 0.5$) and $V_r = 475 \pm 71$ km s^{-1} [note that the physical line-of-sight velocity difference is $\Delta cz/(1+z)$]. These inputs lead to the set of solutions shown as the thick curve in Figure 13, which relates the projection angle to the total mass of the system. The upper and lower thin curves in the figure correspond to $V_r = 404$ km s^{-1}, $R_p = 0.75\ h^{-1}$ Mpc, and $V_r = 546$ km s^{-1}, $R_p = 0.87\ h^{-1}$ Mpc, respectively, showing the range of solutions allowed by the uncertainties in these quantities. To completely solve the model we require the total mass of the system. Since the main Coma cluster completely dominates the NGC 4839 group (see above), the appropriate mass to use is the mass of the main cluster inside the radius corresponding to the true separation R of the two clusters. Since R depends on α, we need to know the mass of the main cluster as a function of radius. For the purposes of this analysis it is sufficient for us to approximate the mass profile as a power law $\log M(<R) \propto \log R$ constrained to pass through the mass esti-

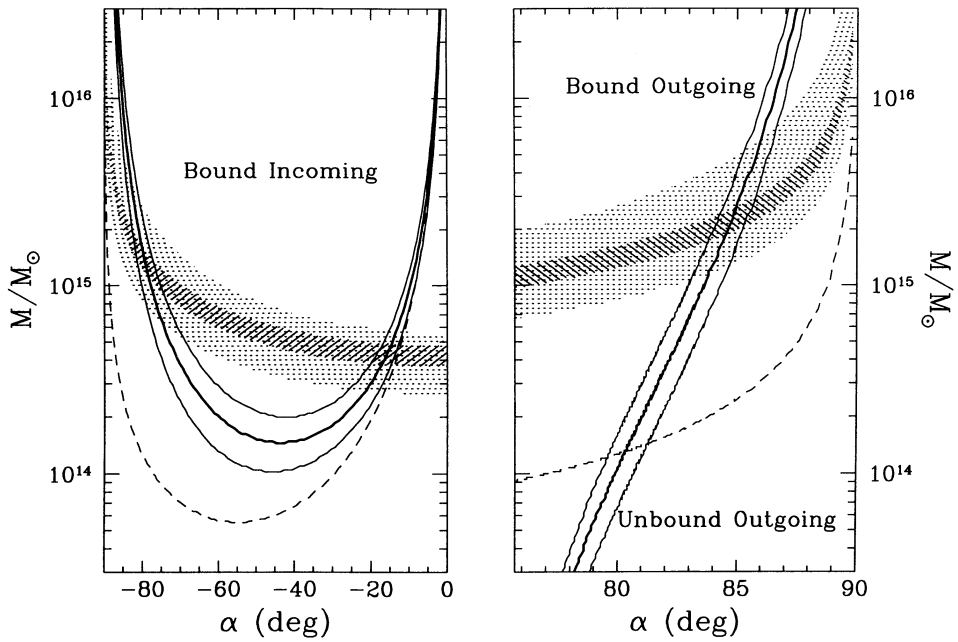

FIG. 13.—Solutions (*thick curve*) of the two-body model for the Coma cluster and the NGC 4839 group, showing the implied total mass as a function of projection angle α. The thin curves show the range of solutions allowed by the uncertainties in the projected separation and relative velocity. The left panel shows the incoming solutions ($\alpha < 0°$), and the right panel the outgoing solutions ($\alpha > 0°$); note that there are no solutions for $0° < \alpha < 76°$. The dashed curves show the mass required to bind the system as a function of α; solutions above this curve are bound and below unbound. The heavily shaded regions show the mass of the Coma cluster inside the radius separating the two subclusters for mass profiles derived assuming mass follows light; the lightly shaded regions show the extreme range of allowed masses.

mates at 0.5 and 2.5 h^{-1} Mpc as given in the previous section. The mass enclosed within the radius of the NGC 4839 group is shown in Figure 13 as a function of projection angle α: the heavy shading corresponds to mass profiles in which mass follows light, while the unconstrained mass profiles are indicated by the lighter shading.

Acceptable solutions for the two-body model thus lie within the regions bounded by the thin curves and the light shading; the preferred solutions are where the thick curves intersect the heavy shading. These solutions are listed in Table 5. There are no unbound solutions—the NGC 4839 group is clearly bound to Coma—but there are three bound solutions, one outgoing (the system has not yet reached turnaround) and two incoming. The bound outgoing solution (BO) has the system aligned at 5^{+1}_{-1} degrees to the line of sight, with the NGC 4839 group lying $8.9^{+2.3}_{-1.0}\,h^{-1}$ Mpc directly behind the Coma cluster and moving away from it at 480^{+70}_{-470} km s^{-1}. The first bound incoming solution (BI1) has the system aligned at 10^{+8}_{-4} degrees to the

TABLE 5

SOLUTIONS OF TWO-BODY MODEL

V_r (km s^{-1})	R_p (Mpc)	Mass Model	α	V (km s^{-1})	R (Mpc)	log ($M/M_\odot$)
		Bound Outgoing Solution				
546.....	0.87	minimum mass	+83°.7	+549	7.89	15.07
475.....	0.81	minimum mass	+83.8	+478	7.50	15.06
475.....	0.81	mass ~ light	+84.8	+477	8.87	15.34
475.....	0.81	maximum mass	+86.0	+476	11.61	15.78
404.....	0.75	maximum mass	+86.2	+10	11.24	15.77
		Bound Incoming Solution 1				
546.....	0.87	minimum mass	−72.0	−574	2.82	14.78
475.....	0.81	minimum mass	−74.8	−492	3.10	14.81
475.....	0.81	mass ~ light	−79.6	−483	4.49	15.14
475.....	0.81	maximum mass	−82.9	−479	6.51	15.55
404.....	0.75	maximum mass	−83.8	−406	6.89	15.58
		Bound Incoming Solution 2				
546.....	0.87	minimum mass	−26.3	−1232	0.97	14.47
475.....	0.81	minimum mass	−21.3	−1305	0.87	14.44
475.....	0.81	mass ~ light	−16.0	−1723	0.84	14.64
475.....	0.81	maximum mass	−13.4	−2055	0.83	14.76
404.....	0.75	maximum mass	−11.2	−2081	0.76	14.73

line of sight, with the NGC 4839 subcluster closer to us than the main Coma cluster by $4.5^{+2.4}_{-1.7}\ h^{-1}$ Mpc and infalling with a velocity of 480^{+90}_{-80} km s^{-1}. The second bound incoming solution (BI2) has the system aligned at 74^{+5}_{-10} degrees to the line of sight, with the main cluster and the NGC 4839 subcluster separated by $0.8^{+0.1}_{-0.1}\ h^{-1}$ Mpc and moving together at a velocity of 1700^{+350}_{-500} km s^{-1}.

We can estimate the relative probability of these solutions if we assume that all dynamically allowed orientations of such a system are equally likely, for then the probability of observing the system at projection angles in the range α_1 to α_2 is proportional to $\sin \alpha_2 - \sin \alpha_1$. Using the allowed ranges of α for the three solutions given in Table 5, we find that probabilities of the BO, BI1, and BI2 solutions are 1%, 15%, and 84%, respectively. Thus, it is far more likely that the NGC 4839 system is incoming rather than outgoing. Of the two incoming solutions, BI2 is significantly favored over BI1. The preferred model for the system, therefore, has the two clusters lying at 74° to the line of sight with a true separation of about 0.8 h^{-1} Mpc and moving together at around 1700 km s^{-1}.

5. DISCUSSION

5.1. *Multiple Substructure and Merging in Coma*

There is now strong evidence from X-ray, optical, and radio observations for multiple substructure and ongoing merging in Coma.

1. The *ROSAT* images by Briel et al. (1992) and White et al. (1993) show that the core of the cluster has an elongated structure joining the two dominant galaxies NGC 4874 and NGC 4889. There is also a secondary concentration producing 6% of the total X-ray emission centered on NGC 4839, 40′ SW of the cluster core (see also Watt et al. 1992). The luminosity and the temperature of this subcluster are similar to those of poor clusters with central dominant galaxies (see Kriss, Cioffi, & Canizares 1983). Evidence that the NGC 4839 group is infalling is provided by the way the X-ray emission trails outward from the cluster core behind NGC 4839. There is also some indication of structure associated with NGC 4911, 20′ SE of the core. Coma has no cooling flow (Edge, Stewart, & Fabian 1992), probably because it has been disrupted in a merger event (McGlynn & Fabian 1984). The lack of strong temperature and metallicity gradients in the X-ray gas in Coma could also be due to a major merger (Watt et al. 1992).

2. The projected galaxy distribution reflects the same structures as the gas, with a secondary peak around NGC 4839 (Mellier et al. 1988) and two clumps centered on NGC 4874 and NGC 4889 in the core (Fitchett & Webster 1987; Baier et al. 1990). Again there is some evidence for a substructure associated with NGC 4911 (Mellier et al. 1988).

3. The analysis of the galaxy velocities presented here clearly shows that the NGC 4839 group is a separate dynamical entity falling into the main cluster (§§ 3.2 and 3.3). It has about 10% the mass of the main cluster (§ 4.2). A simple two-body model (§ 4.3) suggests that it is currently just beginning to penetrate the main cluster and will encounter the cluster core in less than 0.5 Gyr. There is also a significant correlation between the positions and velocities in the cluster core (§ 3.4), with two apparent subclusters separated by only 5′.5 on the sky but by 800 km s^{-1} along the line of sight. In projection these subclusters are associated with the two dominant galaxies NGC 4874 and NGC 4889, although they are offset in velocity by 350 km s^{-1} and 1100 km s^{-1}, respectively.

4. The radio halo of the Coma cluster (Coma C; Venturi, Giovannini, & Feretti 1990; Kim et al. 1990) is one of only a few known; all are in clusters without cooling flows (Burns et al. 1992). Such halos require a source of relativistic electrons, a large-scale magnetic field and in situ acceleration of the electrons. Tribble (1993) suggests that recent merging of subclusters may be necessary to create the conditions required for a persistent cluster-wide radio halo (see also Burns et al. 1994). The NGC 4839 group lies outside the radio halo of Coma, but NGC 4839 itself is a head-tail radio source with the tail pointing away from the main cluster (Venturi et al. 1990), implying that it is falling into the cluster through a fairly dense intracluster medium.

5. There is an excess of early-type galaxies showing evidence of recent star formation in the region of NGC 4839, particularly between NGC 4839 and the cluster core (Caldwell et al. 1993). The star formation in these objects might plausibly have been triggered by interaction with either the mean tidal field or the intracluster medium as they fell into the main cluster. However, as Caldwell et al. note, it is "difficult to maintain that the abnormal-spectrum galaxies are all gravitationally bound members of the SW substructure" since although the 17 abnormal galaxies in the SW region have an appropriate mean velocity of 7288 km s^{-1}, their velocity dispersion is 1262 km s^{-1} (compare the velocity dispersion of 329 km s^{-1} for the NGC 4839 group obtained here). And indeed only three of these galaxies are assigned to the NGC 4839 group by the KMM partition.

5.2. *The Dominant Galaxies*

The properties of the dominant galaxies NGC 4874, NGC 4889, and NGC 4839, especially their extended halos (or lack thereof), are particularly revealing about the substructure and merger history of Coma. Dominant galaxies are believed to form in poor clusters and groups, where the low velocity dispersion facilitates the mergers needed for them to grow (Malumuth 1992, and references therein). In this process an extended halo also forms out of stellar debris from the merger process and tidal stripping of other galaxies. This halo material, which distinguishes a cD from a D galaxy, orbits in the potential well of the entire group and is not bound to the galaxy itself. When the group merges with a rich cluster and is disrupted the halo is destroyed and the cD becomes a D galaxy. Tidal friction causes the very massive ($\sim 10^{13}\ h^{-1}\ M_\odot$) D galaxy to spiral to the cluster center, where it merges with any existing D or cD. Eventually it may reacquire a halo from merger debris and again become a cD.

Schombert (1988) finds clear evidence for extended halos around both NGC 4874 and NGC 4839 and classifies them as cD galaxies. However, there is no evidence for such a halo around NGC 4889, which is therefore classified as a D galaxy. Baier et al. (1990) note several pieces of evidence supporting the interpretation that NGC 4874 is at the bottom of the cluster potential well while NGC 4889 belongs to a recently accreted and disrupted group: (1) NGC 4874 lies at the peak of the X-ray emission and the center of the emission contours at larger scales; (2) the number of galaxies close to NGC 4874 is 50% greater than around NGC 4889; (3) NGC 4874 is a strong radio source coincident with the peak of the extended radio halo of the cluster—by contrast NGC 4889 is not distinguishable in the radio halo. Both galaxies have masses (within 80 h^{-1} kpc) of approximately $1.4 \times 10^{13}\ h^{-1}\ M_\odot$ (Vikhlinin, Forman, & Jones 1994).

With the new information from our analysis of the velocity structure in Coma, one can plausibly argue that, in terms of the evolutionary sequence for dominant galaxies outlined above, NGC 4839 is a cD at the center of the group in which it originally formed, while NGC 4889 is a D galaxy that lost any halo it may have had when it was ejected from its parent group (the core subcluster at 7600 km s^{-1}) in the ongoing merger with the main Coma cluster. The case of NGC 4874 is less clear. It may be a genuine cD at the center of the main cluster, as argued above, though with a peculiar velocity of 300 km s^{-1} with respect to the peak of the galaxy distribution. Alternatively, it may be a D galaxy that is coincidentally projected onto the halo existing at the bottom of the cluster's potential well. In the latter case it may have been ejected from the cluster center in the same encounter that ejected NGC 4889 from the center of its own group.

Thus Coma provides a remarkable case in which various phases in the evolution of D/cD galaxies can be seen simultaneously. Furthermore, the evolutionary stage of the dominant galaxies gives a strong indication of the merger stage of their parent group with the main cluster: the NGC 4839 group is just encountering Coma and is yet to be significantly disrupted, the NGC 4889 "group" has been partially disrupted but has not yet fully merged, while NGC 4874 is the original dominant galaxy of the main cluster, which may have been dislodged from its position at the bottom of the potential well by the encounter with NGC 4889. A similar picture has been proposed by White et al. (1993) to explain the structure in the X-ray gas.

5.3. *Is Coma Pre- or Post-Prandial?*

It has recently been suggested by Burns et al. (1994) that the Coma cluster has just had the NGC 4839 group for lunch: in other words, that the NGC 4839 group has already passed through the core of the main Coma cluster. This is counter to the picture developed above. The main arguments of Burns et al. (and the counterarguments) are as follows.

1. The main cluster's X-ray surface brightness distribution, its isothermal temperature profile, its lack of a cooling flow, and its radio halo all argue strongly for a recent merger event. Burns et al. argue that the NGC 4839 group's passage through the cluster core was that event; however, the arguments of the previous two sections would point to the ongoing merger involving NGC 4889 as a more likely culprit.

2. Burns et al. claim that the X-ray emission around NGC 4839 is unlike that expected for a bound group that has just begun to fall into the main cluster because of the relative flatness of the X-ray profile. They also suggest that the compact X-ray core about NGC 4839 is due to a cooling flow. However, a cooling flow would not survive a merger—indeed, Burns et al. argue that the *lack* of a cooling flow in the main cluster is due to the passage of the NGC 4839 group. The distorted outer X-ray emission contours could more plausibly be interpreted as the trailing plume produced by the group's passage through the intracluster medium of the main cluster (Briel et al. 1992; White et al. 1993).

3. Caldwell et al. (1993) obtained a velocity dispersion of 963 km s^{-1} for galaxies in the SW region of Coma, which Burns et al. correctly point out is inconsistent with a premerger bound group. However, the analysis of this paper shows that there *is* a bound group about NGC 4839 with an appropriately small velocity dispersion; the large value obtained by Caldwell et al. is simply due to the mixture of galaxies from both the main cluster and the NGC 4839 group present in the SW region (see Fig. 9). González-Casado, Mamon, & Salvador-Solé (1995) show using both analytic arguments and numerical simulations that accreted groups and small clusters are tidally disrupted in one cluster crossing (as is the group in the Burns et al. simulation). Thus, the existence of a bound group around NGC 4839 argues strongly against it having already passed through the cluster core.

4. Burns et al. note the existence of a filament of galaxies running NE from Coma toward the Zwicky cluster Zw 1319.9+3135, and suggest that the NGC 4839 group may have fallen into Coma from along this filament, based on a supposed radial velocity for the group that is 100 km s^{-1} smaller than that of the main cluster. However, this filament is part of the Great Wall that extends through Coma to the SW toward the Abell cluster A1367 lying 21 h^{-1} Mpc away. From the results obtained here, the NGC 4839 group has a radial velocity 500 km s^{-1} *greater* than that of the main cluster. Using the position and redshift of A1367 to define the direction of the Great Wall, we find it runs away from Coma toward A1367 at a position angle on the sky of 36° south of west, and at a projection angle α of 19°. This is in good agreement with the observed position angle of the NGC 4839 group and the projection angle corresponding to the favored BI2 solution of our two-body model.

5. Burns et al. note that the distribution and velocities of the early-type galaxies with abnormal spectra found by Caldwell et al. (1993) in the SW region are more like the "spray" of galaxies seen postmerger in their simulation than like the members of a bound group. The present analysis agrees in finding that few of these objects are likely to be members of the NGC 4839 group. However, an alternative explanation for these galaxies is that, while not bound to the NGC 4839 group, they too are recent arrivals at the Coma cluster, onto which they have fallen (like NGC 4839) along the Great Wall from the SW. That such infall occurs is indicated by the broad velocity distribution seen for the bluer galaxies in Figure 12*c*. Moreover early-type *field* galaxies are more likely to have retained their gas reserves than those in the relatively dense environment of the NGC 4839 group. They are, therefore, more plausible candidates for a burst of star-formation. In this context it is clearly of interest to see if there are significant numbers of abnormal-spectrum galaxies at a similar distance from the cluster core but to the NE, arriving from the other side of the Great Wall (this region was not studied by Caldwell et al.).

6. CONCLUSIONS

Inspired by the recent *ROSAT* images of the Coma cluster to reexamine the structure of the galaxy distribution, we have measured redshifts for 243 galaxies using the Hydra multifiber spectrograph at KPNO. Adding these to literature redshifts, we have compiled a catalog of 552 redshifts for Coma based on the photometric sample of Godwin et al. (1983), almost doubling the number of cluster members with redshifts and providing much improved coverage of the regions showing structure in the *ROSAT* images.

The velocity distribution for the 465 cluster members is patently non-Gaussian. We introduce a new test for localized departures from a Gaussian velocity distribution that shows highly significant structure associated with the group of galaxies around NGC 4839, 40′ SW of the cluster core. We apply the KMM mixture-modeling algorithm to the galaxy sample and obtain a robust partition into two subclusters: the main

Coma cluster centered on NGC 4874, with $\overline{cz} = 6853$ km s^{-1} and $\sigma_{cz} = 1082$ km s^{-1}, and a group centered on NGC 4839, with $\overline{cz} = 7339$ km s^{-1} and $\sigma_{cz} = 329$ km s^{-1}.

We use this partition to examine the system's dynamics. Using only the galaxies assigned to the main cluster, we compare the velocity distributions of the red, early-type galaxies and the blue, late-type galaxies and find that $\sigma_{\rm late} \approx 2^{1/2}\sigma_{\rm early}$, suggesting that the late types are freely falling into a virialized main cluster dominated by early types. We obtain a virial mass for the main cluster of $0.9 \times 10^{15}\, h^{-1}\, M_\odot$, in excellent agreement with the best estimates derived from recent X-ray data. The mass of the NGC 4839 group is found to be $0.6 \times 10^{14}\, h^{-1}\, M_\odot$, or about 5%–10% the mass of the main cluster, in accord with their relative richnesses and X-ray luminosities.

Assuming the main cluster and NGC 4839 group follow a linear two-body orbit, we obtain three possible solutions for the system's current state (the ambiguity results from only seeing the system in projection). All three solutions have the NGC 4839 group bound to the main cluster, with the most highly preferred solution having the two clusters lying at 74° to the line of sight at a true (three-dimensional) separation of 0.8 h^{-1} Mpc and moving together at 1700 km s^{-1}.

A closer look at the cluster core shows a highly significant correlation between the galaxy positions and velocities. Plots of the three-dimensional galaxy density and a KMM mixture model for the core suggest the presence of two subclusters: a true central peak close to the projected position of NGC 4874, but with $\overline{cz} \approx 6800$ km s^{-1}, and a secondary peak close to the projected position of NGC 4889, but with $\overline{cz} \approx 7600$ km s^{-1}.

Taking these results in conjunction with other optical, X-ray, and radio observations, we conclude that there is now overwhelming evidence for multiple substructure and ongoing merging in the Coma cluster. We argue that the positions and velocities of the three dominant galaxies, and in particular their possession or lack of an extended halo (i.e., whether they are a cD or a D galaxy), reveal the current status and merger history of the cluster. In our picture, the cD NGC 4839 is at the center of the group in which it originally formed; this group is just falling onto Coma and is yet to be significantly disrupted (contrary to a recent suggestion by Burns et al. 1994). The disturbed X-ray emission and radio halo in the core of the cluster result from the ongoing merger of Coma with a group or cluster of which NGC 4889 was the dominant member; this group has already been partially disrupted (ejecting NGC 4889 and causing the loss of any halo it may have had) but is not yet fully assimilated. NGC 4874 is the true dominant galaxy of the main cluster—it appears to possess an extended halo and lies at the projected peak of the galaxy distribution and the X-ray and radio emission. However, it does not lie at the mean velocity of the main cluster, so it may conceivably have been dislodged from the cluster center in an encounter with NGC 4889. In that case it may be a D galaxy projected onto the halo still residing at the bottom of the cluster potential well.

The future evolution of Coma is likely to be as turbulent as its past. NGC 4874 and NGC 4889 will eventually merge to form a single cD in the core of the cluster, only to be disturbed once more by the impact of the NGC 4839 group. The final dynamical relaxation of the cluster is indefinitely postponed.

We thank Simon White for suggesting follow-up of the *ROSAT* results and Gus Oemler for assistance with the observations. Christina Bird kindly provided us with the KMM code and helpful advice on how to use it. Agris Kalnaj made suggestions on the use of density maps to probe for substructure, which materially improved our analysis.

REFERENCES

Ashman, K. M., & Bird, C. M. 1994, AJ, 108, 2348
Bahcall, J. N., & Tremaine, S. 1981, ApJ, 244, 805
Baier, F. W., Fritze, K., & Tiersch, H. 1990, Astron. Nachr., 311, 89
Beers, T. C., Flynn, K., & Gebhardt, K. 1990, AJ, 100, 32
Beers, T. C., Forman, W., Huchra, J. P., Jones, C., & Gebhardt, K. 1991, AJ, 102, 1581
Beers, T. C., Geller, M. J., & Huchra, J. P. 1982, ApJ, 257, 23
Bird, C. M. 1994, AJ, 107, 1637
———. 1995, ApJ, 445, L81
Biviano, A., Durret, F., Gerbal, D., Le Fèvre, O., Lobo, C., Mazure, A., & Slezak, E. 1995, A&AS, 111, 265
Briel, U. G., Henry, J. P., & Böhringer, H. 1992, A&A, 259, L31
Burns, J. O., Roettiger, K., Ledlow, M., & Klypin, A. 1994, ApJ, 427, L87
Burns, J. O., Sulkanen, M. E., Gisler, G. R., & Perley, R. A. 1992, ApJ, 388, L49
Caldwell, N., Rose, J. A., Sharples, R. M., Ellis, R. S., & Bower, R. G. 1993, AJ, 106, 473
Colless, M. M. 1987, Ph.D. thesis, Univ. Cambridge
Colless, M. M., & Hewett, P. C. 1987, MNRAS, 224, 453
Danese, L., De Zotti, G., & di Tullio, G. 1980, A&A, 82, 322
Dressler, A., & Shectman, S. 1988, AJ, 95, 985
Edge, A. C., Stewart, O. C., & Fabian, A. C. 1992, MNRAS, 258, 177
Fitchett, M., & Webster, R. 1987, ApJ, 317, 653
Giovannini, G., Feretti, L., Venturi, T., Kim, K. T., & Kronberg, P. P. 1993, ApJ, 406, 399
Godwin, J. G., Metcalfe, N., & Peach, J. V. 1983, MNRAS, 202, 113 (GMP)
González-Casado, Mamon, G. A., & Salvador-Solé, E. 1994, ApJ, 433, L61
Gregory, S. A., & Thompson, L. A. 1984, ApJ, 286, 422
Heisler, J., Tremaine, S., & Bahcall, J. N. 1985, ApJ, 298, 8
Huchra, J. P. 1985, in ESO Workshop Proc. No. 20, The Virgo Cluster, ed. O. G. Richter & B. Binggeli (Munich: ESO), 181
Hughes, J. P. 1989, ApJ, 337, 21
Kent, S. M., & Gunn, J. E. 1982, AJ, 87, 945
Kim, K. T., Kronberg, P. P., Dewdney, P. E., & Landecker, T. L. 1990, ApJ, 355, 29
Kriss, G. A., Cioffi, D. S., & Canizares, C. R. 1983, ApJ, 272, 49
Malumuth, E. M. 1992, ApJ, 386, 420
McGlynn, T. A., & Fabian, A. C. 1984, MNRAS, 208, 709
McLachlan, G. J., & Basford, K. E. 1988, Mixture Models: Inference and Applications to Clustering (New York: Marcel Dekker)
Mellier, Y., Mathez, G., Mazure, A., Chauvineau, B., & Proust, D. 1988, A&A 199, 67
Merritt, D. 1987, ApJ, 313, 121
Merritt, D., & Gebhardt, K. 1996, in Proc. XXIX Rencontre de Moriond, Clusters of Galaxies, ed. F. Durret, A. Mazure, & J. Trân Thanh Vân, in press
Merritt, D., & Saha, P. 1993, ApJ, 409, 75
Merritt, D., & Tremblay, B. 1994, AJ, 108, 514
Peebles, P. J. E. 1971, Physical Cosmology (Princeton: Princeton Univ. Press)
Press, W. H., Flannery, B. P., Teukolsky, S. A., & Vetterling, W. T. 1986, Numerical Recipes (Cambridge: Cambridge Univ. Press)
Schombert, J. M. 1988, ApJ, 328, 475
The, L. S., & White, S. D. M. 1986, AJ, 92, 1248
Tonry, J. L., & Davis, M. 1979, AJ, 84, 1511
Tribble, P. 1993, MNRAS, 263, 31
van Haarlem, M. P., Cayón, L., de la Cruz, C. G., Martínez-González, E., & Rebolo, R. 1993, MNRAS, 264, 71
Venturi, T., Giovannini, G., & Feretti, L. 1990, AJ, 99, 1381
Vikhlinin, A., Forman, W., & Jones, C. 1994, ApJ, 435, 162
Watt, M. P., Ponman, T. J., Bertram, D., Eyles, C. J., Skinner, G. K., & Willmore, A. P. 1992, MNRAS, 258, 738
White, S. D. M., Briel, U. G., & Henry, J. P. 1993, MNRAS, 261, L8